Published online 11 September 2017 *Nucleic Acids Research, 2017, Vol. 45, No. 20* **11725–11742**
doi: 10.1093/nar/gkx782

The nuclear mitotic apparatus protein NuMA controls rDNA transcription and mediates the nucleolar stress response in a p53-independent manner

Swaathi Jayaraman[1,2,†], Shirisha Chittiboyina[1,†], Yunfeng Bai[1], Patricia C. Abad[1], Pierre-Alexandre Vidi[1], Cynthia V. Stauffacher[2,3] and Sophie A. Lelièvre[1,3,*]

[1]Department of Basic Medical Sciences, Purdue University, West Lafayette, IN 47907-2026, USA, [2]Department of Biological Sciences, Purdue University, West Lafayette, IN 47907-2026, USA and [3]Center for Cancer Research, Purdue University, West Lafayette, IN 47907-2026, USA

Received March 28, 2017; Revised August 23, 2017; Editorial Decision August 24, 2017; Accepted August 30, 2017

ABSTRACT

The nuclear mitotic apparatus protein, NuMA, is involved in major cellular events such as DNA damage response, apoptosis and p53-mediated growth-arrest, all of which are under the control of the nucleolus upon stress. Proteomic investigation has identified NuMA among hundreds of nucleolar proteins. Yet, the precise link between NuMA and nucleolar function remains undetermined. We confirm that NuMA is present in the nucleolus and reveal redistribution of NuMA upon actinomycin D or doxorubicin-induced nucleolar stress. NuMA coimmunoprecipitates with RNA polymerase I, with ribosomal proteins RPL26 and RPL24, and with components of B-WICH, an ATP-dependent chromatin remodeling complex associated with rDNA transcription. NuMA also binds to 18S and 28S rRNAs and localizes to rDNA promoter regions. Downregulation of NuMA expression triggers nucleolar stress, as shown by decreased nascent pre-rRNA synthesis, fibrillarin perinucleolar cap formation and upregulation of $p27^{kip1}$, but not p53. Physiologically relevant nucleolar stress induction with reactive oxygen species reaffirms a p53-independent $p27^{kip1}$ response pathway and leads to nascent pre-rRNA reduction. It also promotes the decrease in the amount of NuMA. This previously uncharacterized function of NuMA in rDNA transcription and p53-independent nucleolar stress response supports a central role for this nuclear structural protein in cellular homeostasis.

INTRODUCTION

The stabilizing and controlling functions of the nuclear mitotic apparatus protein (NuMA) within the chromatin, the nuclear matrix and at the spindle poles (1–3) suggest management capabilities for this structural protein. Whereas essential roles for NuMA in spindle pole formation and in asymmetric cell division are well documented (4–6), knowledge regarding its functions in the cell nucleus remains sparse and somewhat eclectic. Reports describe the participation of NuMA in chromatin organization associated with cellular differentiation (1,7) and in nuclear architecture, including splicing factor speckles distribution and RNP network integrity (8–10). An increasing number of studies have revealed a specific involvement of NuMA in several nuclear pathways, such as the early phase of chromatin response to DNA damage (11,12), the early phase of nuclear changes linked to apoptosis (13) and downstream p53 pathways in which NuMA acts as a coactivator promoting p53-mediated transcription of certain target genes (14,15). All of these pathways play a pivotal role in the maintenance of cellular homeostasis.

A body of literature has shed light on the importance of the nucleolus, the node of ribosomal synthesis, as a major guardian of cellular homeostasis (16). In response to DNA damage, oxidative stress and other stimuli that threaten homeostasis, the nucleolus produces a stress response with impact on the regulation of cell cycle progression, senescence and apoptosis (17). This essential function of the nucleolus likely explains the plethora of proteins identified in this nuclear compartment, most of which are not directly involved in ribosomal biogenesis *per se* (18,19). Oddly, the observation of NuMA immunostaining with regular microscopy reveals a widespread distribution in the nucleus of most cell types that appears to exclude the nucleolus (11,20), although proteomic analyses of the human nucleolus have indicated NuMA as a putative nucleolar protein

*To whom correspondence should be addressed. Tel: +1 765 496 7793; Fax: +1 765 494 0781; Email: lelievre@purdue.edu
†These authors contributed equally to the paper as first authors.

(18,19). The predicted presence of NuMA in the nucleolus, and the participation of this protein in the regulation of mechanisms controlling homeostasis and associated with nucleolar stress response called for further investigation.

Here we confirm that NuMA is present in the nucleolus and show that this protein interacts with ribosomal DNA (rDNA), ribosomal RNA, B-WICH proteins involved in rDNA transcription and ribosomal proteins. Like other pillar proteins of the nucleolus, NuMA may respond to nucleolar stress by forming perinucleolar caps. We further demonstrate that NuMA regulates the levels of rRNAs and that the absence of NuMA triggers nucleolar stress via a p53-independent pathway. Considered structural in nature, the coiled-coil protein NuMA appears as a new kind of nucleolar protein that orchestrates the response to stressful stimuli.

MATERIALS AND METHODS

Cell culture

Non-neoplastic S1 HMT-3522 breast epithelial cells (21) were seeded at 2.4×10^4 cells/cm^2 and cultured between passages 52 and 60 in H14 medium [Dulbecco's modified Eagle's medium (DMEM)/F12 (Invitrogen), supplemented with 30.3 IU/ml prolactin (Sigma-Aldrich), 100 μg/ml insulin (Sigma-Aldrich), 2.6 μg/ml sodium selenite (BD Biosciences), 2.67×10^{-5} μg/ml β-estradiol (Sigma-Aldrich), 0.5 mg/ml hydrocortisone (Sigma-Aldrich), 20 mg/ml transferrin (Sigma-Aldrich) and 20 mg/ml Epidermal Growth Factor (EGF) (BD Biosciences)] as previously described (1). Non-neoplastic MCF10A cells were seeded at 2.4×10^4 cells/cm^2 in H14 medium similar to that of S1 cells. To induce cell cycle exit, EGF was omitted from the medium for 48 h (with cultures ended at day 6) to 72 h (with cultures ended at day 10). S1-derived malignant T4–2 HMT-3522 cells (22) were seeded at 1.16×10^4 cells/cm^2 and cultured between passages 28 + 4 and 28 + 20 in H14 medium without EGF. MCF7 cells were cultured in DMEM supplemented with 10% fetal bovine serum (FBS) (American Type Culture Collection, ATCC, Manassas, VA). P53-null MDA-MB-157 cells (23; ATCC) were seeded at 2.5×10^4 cells/cm^2 as per ATCC guidelines, in DMEM/F12 medium supplemented with 10% FBS. Cultures of malignant cells were routinely used after four to 6 days. To selectively inhibit rDNA transcription, cells were treated for 4 h in the presence of 0.08 μg/ml Actinomycin D (Sigma-Aldrich) (24) or in the presence of 0.3 μM of doxorubicin (Sigma-Aldrich) (25) for 6 h. To induce oxidative stress, cells were treated for 4 h with 250 μM hydrogen peroxide (H_2O_2).

Antibodies

Mouse monoclonal antibodies against Lamin B1 (1/10 000 dilution, NA12, Calbiochem), nucleolin (C23) (1 μg/ml for western blot and 4 μg/ml for immunostaining, sc-8031, Santa Cruz Biotechnology), NuMA (1/2, clone B_1C_{11}, a kind gift from Dr Jeffrey Nickerson, University of Massachusetts, Worcester, MA, USA), ProMyelocytic Leukemia (PML) (4 μg/ml, sc-966, Santa Cruz Biotechnology) and α-Tubulin (1/500 dilution, T5168, Sigma-Aldrich); rabbit polyclonal antibodies against antioxidant protein 2 (AOP2) (1 μg/ml for western blotting; 5 μg/ml for immunostaining, ab59543, Abcam), fibrillarin (1 μg/ml for western blot and 4 μg/ml for immunostaining, sc-25397, Santa Cruz Biotechnology), Lamin B (1/10 000 dilution; ab16048 Abcam), nuclear myosin 1 (NM1) (0.8 μg/ml, M3567, Sigma-Aldrich), nucleophosmin (B23) (0.5 μg/ml for western blot; 2 μg/ml for immunostaining, sc-5564, Santa Cruz Biotechnology), $p27^{kip1}$ (1 μg/ml for western blot; 2 μg/ml for immunostaining, DB017, Delta Biolabs), p53 (1 μg/ml, 9284, Cell Signaling), p53 binding protein 1 (53BP1) (1 μg/ml, ab36823, Abcam), Ribosomal Protein (RP) L26 (RPL26) (1 μg/ml for western blot and 10 μg/ml for immunostaining, R0655, Sigma-Aldrich), RPS3 (1/1000 dilution, 2579, Cell Signaling), RPL24 (4 μg/ml, ab126172, Abcam), large subunit of RNA polymerase I (RPA194) (1 μg/ml, sc-28714, Santa Cruz) and SNF2h (2 μg/ml for western blot and 4 μg/ml for immunostaining, ab3749, Abcam).

Nucleoli isolation

Isolation of nucleoli from nuclear extracts was carried out as described previously (26). Briefly, malignant T4–2 HMT-3522 cells in 2D culture at 90% confluency were rinsed thrice in pre-warmed phosphate-buffered saline (PBS) buffer. The cells were detached by the addition of 0.25% Trypsin-1 mM ethylenediaminetetraacetic acid (EDTA) (*In Vitro* Corporation) at 37°C for 5 min, and harvested in pre-warmed DMEM medium containing 10 mg/ml soybean trypsin inhibitor (Sigma-Aldrich) and centrifuged at 200 *g* for 10 min. The pellet was rinsed thrice in ice-cold PBS solution and centrifuged for 5 min at 4°C and resuspended in Buffer A [10 mM HEPES, pH 7.9 (Sigma-Aldrich), 10 mM KCl (Mallinckrodt), 1.5 mM $MgCl_2$ (Sigma-Aldrich), 0.5 mM DTT (Sigma-Aldrich)] containing protease inhibitor cocktail (PIC) (Sigma-Aldrich) for 5 min on ice. Cells were lysed using a dounce homogenizer with 50 upward and downward strokes and centrifuged at 450 *g* for 10 min at 4°C. The pellet corresponding to enriched, but not highly pure, nuclei was resuspended in S1 solution [0.2 M Sucrose (Sigma-Aldrich), 10 mM $MgCl_2$] containing PIC and layered on top of S2 solution [0.35 M Sucrose, 0.5 mM $MgCl_2$] containing PIC, and centrifuged at 1250 *g* for 5 min at 4°C. The resulting cleaner nuclear pellet was mixed in S2 solution and sonicated by six cycles of 10 s bursts with intermittent cooling on ice using a sonic dismembrator (Fisher Scientific). The sonicated sample was layered on top of S3 solution [0.88 M Sucrose, 0.5 mM $MgCl_2$] containing PIC and centrifuged at 2450 *g* for 10 min at 4°C. The final pellet corresponds to highly purified nucleoli. Total protein extracts and purified nucleoli fractions were separated on a sodium dodecyl sulfate-polyacrylamide (SDS-PAGE) gel, transferred onto a nitrocellulose membrane (Bio-Rad) and analyzed by immunoblot.

Electron microscopy and immunolabeling

Cells cultured in 35 mm dishes were fixed with 3% paraformaldehyde and 0.1% glutaraldehyde in 20 mM Na-Na_2 phosphate buffer containing 150 mM NaCl, pH 7.4 for

1 h and rinsed in PBS-20 mM Na-Na_2 phosphate buffer containing 150 mM NaCl, pH 7.4. The cells were incubated in PBS containing 50 mM ammonium chloride to quench free aldehyde groups followed by incubation in PBS-1% non-fat dry milk to block non-specific protein sites. Following a brief rinse in PBS, cells were incubated either without primary antibody or with NuMA B_1C_{11} antibody diluted in goat serum (1:1 ratio) at 4°C overnight. The next day, cells were rinsed three times in PBS-BT buffer [PBS containing 1% bovine serum albumin (BSA)] and incubated with secondary antibodies (Nanogold gold-antimouse immunoglobulin G (IgG) and Fab conjugate) diluted 1:50 in PBS-BT buffer containing 1% goat serum, for 1 h at room temperature. Following three washes in PBS, samples were fixed with 1% glutaraldehyde in PBS, at room temperature. Incubation with 50 mM ammonium chloride in PBS was used to quench free aldehyde groups. Cells were then washed in PBS and double distilled water (ddH2O) followed by incubation with GoldEnhance kit #2113 (Nanoprobes, Inc.), based on the manufacturer's protocol to amplify the gold signal and rinsed in ddH2O. Secondary fixation was performed in the presence of equal volumes of 1% reduced osmium (OsO_4) and 1.5% $K_3Fe(CN)_6$ for 30 min at room temperature, and cells were rinsed in ddH_2O. Embedding of the cells was carried out in different ratios of Epon/Ethanol mixtures. Finally, inverted capsules filled with Epon were set on the embedded cells and allowed to polymerize for 48 h at 60°C. Thin sections of cell blocks were made for subsequent visualization by transmission electron microscopy (TEM).

Nucleolar localization signal analysis

The presence of nucleolar localization signal (NoLS) in full length NuMA sequence (residues 1–2101) was analyzed using the nucleolar localization sequence detector (NoD) web server (http://www.compbio.dundee.ac.uk/www-nod) (27). The NoD server integrates algorithms from Stuttgart Neural Network Stimulator and human-trained NoLS prediction models (27). If the average NoLS output score of eight consecutive amino acids is at least 0.8 the NoD server returns two outputs: (i) the primary sequence of the protein with the predicted NoLS highlighted in red and (ii) a graph that displays, on the X-axis, the entire protein sequence with the position of the predicted NoLS(s) highlighted in the pink region of the graph and, on the Y-axis, the NoLS prediction score for every 20-residue window in the protein.

Immunofluorescence staining

Immunofluorescence staining was performed as previously described (1), with secondary antibodies Fluorescein isothiocyanate (FITC)-conjugated donkey antirabbit IgG (1:300, 711–096-1520, Jackson Immunoresearch), Alexa Fluor 568-conjugated goat antimouse IgG (6.6 μg/ml, A11004, Invitrogen) or Alexa Fluor 568-goat antirabbit IgG (4 μg/ml, A11011, InVitrogen).

Immunoprecipitation

Preparation of nuclear extracts followed by coimmunoprecipitation (coIP) was performed using the universal magnetic coIP kit (Active Motif) based on the manufacturer's instructions. Briefly, for each IP reaction, 1–1.5 mg of the nuclear extracts and 10–15 μg of either mouse monoclonal NuMA antibody (NA08, Calbiochem), rabbit NuMA antibody (A301–510A, Bethyl Laboratories), ChromPure Mouse (015–000-003, Jackson ImmunoResearch) or rabbit (011–000-003, Jackson ImmunoResearch) whole IgGs were combined in a final volume of 1–1.5 ml of the IP buffer and incubated overnight at 4°C. The antibody-bound fraction was incubated with 50–75 μl of magnetic dynabeads (Invitrogen) for 1 h at 4°C followed by four rapid washes with coIP buffer. Finally, the beads were resuspended in 40–60 μl of 2× protein loading buffer. The IP samples were separated on a SDS-PAGE gel, transferred onto a nitrocellulose membrane and analyzed by immunoblot.

Chromatin immunoprecipitation

The chromatin immunoprecipitation (ChIP) protocol was modified from Lee *et al.* (28). T4–2 cells (4×10^7) cultured in 150 mm dishes were cross-linked with a formaldehyde solution (50 mM HEPES-KOH, pH7.5; 100 mM NaCl; 1 mM EDTA; 0.5 mM ethylene glycol-bis(β-aminoethyl ether)-N,N,N',N'-tetraacetic acid) (EGTA; 11% formaldehyde) for 10 min and quenched with 0.125 M Glycine. After rinsing thrice with PBS, cells were harvested by scraping into a 15 ml falcon tube and kept at −80°C until used. Dynabeads Protein G (80 μl; InVitrogen) were washed thrice in 1 ml blocking buffer (PBS with 0.5% BSA (Sigma-Aldrich) before splitting the volume equally for separate incubation with 2 μg rabbit NuMA antibody or whole IgG at 4°C for 6 h. Antibody/IgG covered-beads were resuspended in 100 μl blocking buffer. Cells were thawed on ice and mixed with 10 ml lysis buffer (10 mM Tris-HCl, pH 7.5; 10 mM NaCl; 3 mM $MgCl_2$; 0.5% IGEPAL; 1 mM phenylmethylsulfonyl fluoride (PMSF) by gently pipetting and inverting the tubes for 5 min, before centrifuging at 700 *g* for 5 min. The cell lysis step was repeated two more times and the cell pellet was finally resuspended in 830 μl pre-IP dilution buffer (10 mM Tris-HCl, pH 7.5; 150 mM NaCl; 3 mM $MgCl_2$; 1 mM CaCl2; 4% IGEPAL; 0.8% SDS, 1 mM PMSF; PIC [Roche]). Tubes were left on ice for 5 min before dilution with 3× volumes of IP dilution buffer (20 mM Tris-HCl, pH 8; 2 mM EDTA; 1% Triton X-100; 150 mM NaCl, PIC). Cells in solution were then subjected to sonication (35 bursts, output 10 Watts, with 20 s per burst at 90 s intervals on ice). The sonicated solution was spun down at 16 000 *g* for 10 min to remove the cell debris, and 50 μl of sample was kept as input control. The remainder of the supernatant was equally split into two parts for incubation with antibody-coated beads or IgG-coated beads on a rotating wheel at 4°C and for 2 h. The beads were collected and gently washed with 700 μl ChIP wash buffer 1 (20 mM Tris-HCl, pH 8; 2 mM EDTA; 1% Triton X-100; 150 mM NaCl; 1 mM PMSF), followed by buffer 2 (20 mM Tris-HCl, pH 8; 2 mM EDTA; 1% Triton X-100; 0.1% SDS; 500 mM NaCl; 1 mM PMSF) and buffer 3 (10 mM Tris-HCl, pH 8; 1 mM EDTA; 0.25M LiCl; 0.5% IGEPAL; 0.5% deoxycholate) for 5 min at room temperature. The beads were then transferred to a new tube to perform a wash with 700 μl

of Tris-EDTA buffer. The collected beads were resuspended in 100 μl of elution buffer (25 mM Tris-HCl, pH 7.5; 10 mM EDTA; 0.5% SDS), incubated at 65°C for 30 min and trapped using a magnetic bar to collect the solution. After repeating the elution step, reverse cross-linking was carried out by incubating the ChIP products and input sample at 65°C overnight, followed by treatment with 0.2 μg/ml of RNaseA for 2 h at 37°C and 0.2 μg/ml proteinase K at 55°C for another 2 h. Finally, samples were purified with Qiagen PCR Purification Kit and resolved in 50 μl elution buffer. The ChIP products were analyzed by real-time PCR on ABI 7300 with Sybr green (Applied Biosystems). The sequence of primer pairs targeting different regions of the human ribosomal DNA (rDNA) (pro-1, H4, H8, H13 and H18) and the length of PCR products were as described previously (29). The PCR reaction system was a 20 μl volume composed of 1 μl of ChIP product, 8 μl of water, 0.5 μl each of the forward and reverse primers (10 μM) and 10 μl of Sybr green. The PCR conditions were 55°C for 2 min, 95°C for 10 min, 95°C for 10 s, annealing at 58°C for 1 min (40 cycles), extension at 72°C for 10 s. PCR product specificity was assessed through melt curve. Amplification of ChIP input was used as an internal control. To eliminate the difference of antibody (and IgG) binding efficiency at distinct regions and the variations of enrichment folds among the biological replicates, two steps of normalization were carried out at each individual region during statistical analysis. First, the enrichment of NuMA at different rDNA regions relative to IgG was obtained by normalizing the input percent of NuMA to that of IgG. Relative expression between the samples was calculated by the comparative Cq method. Second, the relative enrichment of NuMA at different regions was further normalized to that at region H4.

RNABindR and BindN analysis

The presence of RNA-interacting residues in full length NuMA sequence (residues 1–2101) was analyzed by the RNA web-based servers BindN and RNABindR (30,31). Both servers returned as output the input sequence with each amino acid receiving either a positive or negative symbol, denoting the particular residue as either a RNA-interacting or non-interacting residue, respectively. To identify RNA-interacting residues the output sequences from the two servers were aligned; only amino acid residues that were assigned a positive sign by both servers were considered as 'potential' RNA-interacting residues.

RNA immunoprecipitation

The RNA immunoprecipitation protocol was adapted from Obrdlik *et al*. (32). Briefly, T4–2 cells treated with or without 50 μg/ml of cycloheximide (Sigma-Aldrich) for 3 h, a drug that inhibits protein translation, were scrapped in ice-cold PBS-PI solution prepared in diethylpyrocarbonate (DEPC, Sigma-Aldrich) water and centrifuged at 1500 *g* for 5 min. The cell pellet was resuspended in 4 ml ice-cold PBS buffer containing 0.2% Nonidet P-40, 1 mM PMSF and 40 U/ml recombinant RNAsin ribonuclease inhibitor (Promega), lysed using a dounce homogenizer (50 strokes/ml) and centrifuged at 800 *g* for 10 min at 4°C. The resulting nuclear pellet was separated from the supernatant (the latter fraction represents soluble proteins from the cytoplasmic fraction and is called soluble extract). The nuclear pellet was resuspended in 1 ml of ice-cold DEPC-PBS containing 1 mM PMSF and 40 U/ml RNaseOut, sonicated using a Sonic Dismembrator (Fisher Scientific) and centrifuged at 14 000 *g* for 30 min at 4°C to obtain the nuclear extract. Nuclear and soluble extracts were precleared with 50 μl protein G sepharose (GE Healthcare) pre-equilibrated in DEPC-PBS and incubated for 1 h with rabbit antibodies against NuMA or whole IgG (1 μg/sample). After incubation, samples were supplemented with 20 μl PBS-equilibrated protein G sepharose for 1 h at 4°C, with constant agitation to precipitate the antibodies. After three washes with 50 volumes (relative to G sepharose beads) of mild RIPA buffer (PBS containing 0.4% Nonidet P-40, 0.02% Na deoxycholate, 1 mM PMSF and 20 U/ml RNasin inhibitor), the immunoprecipitated RNA was extracted with Trizol reagent (Ambion) according to the manufacturer's instructions. The extracted RNA was incubated with 2 U DNase I (New England Biolabs) for 30 min at room temperature. The reaction was stopped by addition of 2 mM EDTA and incubation at 75°C for 10 min. The DNAse-treated RNA sample was reverse-transcribed into cDNA using the Iscript™ DNA synthesis kit (Bio-Rad). Briefly, a 20 μl reaction volume composed of 1 μg of RNA, DEPC water, 1 μl of reverse transcriptase and 4 μl of 5X buffer was amplified into cDNA using the PCR conditions: 5 min at 25°C, 30 min at 42°C and 5 min at 82°C (Bio-Rad thermocycler).The cDNA was analyzed with real-time PCR on ABI 7300 with Sybr green (Applied Biosystems) using conventional PCR primer combinations specific for human 45S pre-rRNA (sequences obtained from references 33 and 34), 28S rRNA and 18S rRNA (obtained from Maximbio Inc.). The real-time reaction conditions were 20 μl volume composed of 2 μl of cDNA, 6 μl water, 1 μl each of the forward and reverse primers (10 μM) and 10 μl of Sybr green. The real-time PCR conditions were: step 1, 50°C for 2 min; step 2, 95°C for 10 min; step 3, 95°C for 15 s, 50°C for 30 s, 72°C for 1 min (40 cycles) followed by dissociation curve. The DNAse-treated non-reverse-transcribed RNA samples were also screened by real-time PCR for the above rRNAs to confirm lack of genomic DNA contamination. Amplification of PUM1 gene was used as an internal control (35). Relative expression between the samples was calculated by the comparative C_q method.

Transfection of siRNAs

Cell cultures at 20–30% confluency were transfected with 25 nM NuMA siRNA and non-targeting siRNA (GE Dharmacon) using Lipofectamine transfection reagent (ThermoFisher Scientific) for 24 h. Cells were maintained in culture post-transfection for an additional 6 days for S1 and MCF10A cells and an additional 4 days for T4–2, MCF7 and MDA-MB-157 cells with regular medium change every 2 to 3 days to allow enough time for the reduction of the level of NuMA protein (1). Protein extracts were obtained by processing the cells in PBS with 4% SDS as described earlier (1).

FUrd staining

A 100 mM stock solution of 5-fluorouridine (5-FUrd; Sigma-Aldrich) was prepared in DMSO, aliquoted under N_2 gas flow, and stored at 4°C (up to one month). On the day of the experiment, cells were treated with 2 nM 5-FUrd (final concentration) for 15 min in the cell culture incubator (37°C, 5% CO_2). Cells were then briefly washed with cold PBS once and fixed in 4% paraformaldehyde for 15 min, followed by incubation in 1% Triton X-100 in immunofluorescence buffer (1) for 5 min. After three washes with 2.5 M glycine in PBS, cells were blocked in 10% goat serum for 1 h and incubated with mouse monoclonal antibody against halogenated uridine (1/200 dilution, B2531, Sigma-Aldrich) to detect 5-FUrd, followed by incubation with 6.7 μg/ml Alexa-Fluor 568-conjugated goat antimouse IgG (InVitrogen) for 1 h each, according to standard immunostaining protocol (1). For quantification, measurements were performed on randomly selected nucleolar regions from images taken with a fluorescence microscope. To compare cells with NuMA expression and cells silenced for NuMA, the signal was quantified using Image*J* software from the National Institutes of Health (NIH) (http://rsbweb.nih.gov/ij/). The approach followed previously published methods (36). The average of the mean grey values in NuMA expressing (NuMA+) cells was determined, and defined as 100% of signal. The average of the mean grey values measured in NuMA silenced cells (NuMA−) was expressed proportionally to that of the normalized value from NuMA expressing cells. To compare several treatment conditions, internal fluorescence level was taken into account by calculating the ratio of mean grey values of the nucleolar regions over the mean grey values of the nucleoplasm (without the nucleolus). Briefly, the nucleus was outlined and the mean grey intensity of FUrd was obtained. Within the same image the nucleolus was outlined and the mean gray intensity of FUrd was obtained. Nucleoplasmic intensity of FUrd was calculated as FUrd intensity in the nucleus minus FUrd intensity in the nucleolus. The area of the nucleoplasm was determined by subtracting the area of the nucleolus from the area of the nucleus. Finally, the ratio of FUrd staining intensity in the nucleolus compared to the nucleoplasm was calculated as 'FUrd intensity in the nucleolus/area of the nucleolus) over (FUrd intensity in the nucleoplasm/area of the nucleoplasm)'.

Image acquisition and analysis

Immunofluorescence images were captured using an Olympus IX70 fluorescence microscope, and the images were processed using the image analysis *ImageJ*.

Statistical analysis

Statistical analysis was performed using Prism (GraphPad Software). Data are presented as means ± s.e.m. We used unpaired Student's *t*-test for comparison of two samples, analysis of variance (ANOVA) with Tukey's post hoc test for comparison of more than two samples, and one-sample *t*-test when the analysis was done relative to a control used as standard. *P*-value levels are indicated in the figure legends. $P < 0.05$ was considered significant.

RESULTS

NuMA is present in the nucleolus and responds to nucleolar stress

To explore the link between NuMA and the nucleolus we used non-neoplastic and malignant cells. The protein NuMA was present in the nucleolar fractions along with other nucleolar proteins, such as the nucleolar marker fibrillarin and the large ribosome subunit protein RPL26. The absence of the cytoplasmic marker α-Tubulin and the nucleoplasmic marker p53 binding protein 1 (53BP1) confirmed the lack of cross-contamination from other cellular compartments during the preparation of the nucleoli (Figure 1A). When visualized by TEM, the organization of nucleoli is divided into fibrillar centers (FCs), dense fibrillar components (DFCs) and granular components (GCs), where different stages of ribosome biogenesis take place (37,38). Electron micrographs indicated the presence of NuMA predominantly in the DFCs, the sites of rDNA transcription and rRNA processing, and the GCs, the sites of final maturation of pre-ribosomal ribonucleoproteins and of ribosomal subunits assembly (i.e. 11 out of 16 FCs analyzed lacked NuMA, while all DFCs/GCs showed the presence of NuMA) (Figure 1B and C). The possibility of the presence of NuMA in the nucleolus was reinforced by the detection of a NoLS in the C-terminus of the protein based on the NOD predictor. The presence of NoLS was predicted in the nucleolar protein NOA36, but not in the nucleolar protein Nucleolin as previously reported (39,40). No NoLS was found in 53BP1, a nuclear protein that has never been described in the nucleolus (Supplementary Figure S1). These preliminary findings suggest that the presence of NuMA in the nucleolus may not be a mere coincidence.

Many proteins involved in ribosome biogenesis relocate to the nucleolar periphery (forming perinucleolar caps) or translocate from the nucleolus to the nucleoplasm upon nucleolar stress induced by inhibiting rDNA transcription with low concentration (0.08 μg/ml) of actinomycin D (24,41–43). Nucleolar stress refers to the cellular response that arises from defects in the ribosome biogenesis process; it occurs naturally when triggered by imbalances in nutrient supply, growth stimuli, cellular energy status and elevated levels of reactive oxygen species (ROS), all of which ultimately affect cellular homeostasis (17). Inhibition of rDNA transcription by actinomycin D treatment in S1 cells significantly altered the distribution of NuMA in 39.68% ± 3.67 of the cell population, as illustrated by the formation of perinucleolar caps and intranucleolar rings (least frequent). These patterns were rarely observed in the vehicle (DMSO)-treated cells (4.51% ± 0.98 of the cell population) (Figure 2A and B). Perinucleolar caps were also significantly induced for nucleolar fibrillarin, a usual marker of nucleolar stress, upon actinomycin D treatment (42.00% ± 2.31 in treated versus 1.83% ± 0.17 untreated cells) (Figure 2A and B). The PML protein that has no reported role in ribosome biogenesis, but was shown to participate in p53 stabilization by controlling MDM2 sequestration in the nucleolus (44), did not redistribute upon actinomycin D treatment. Additional experiments with another rDNA transcription inhibitor, doxorubicin (0.3 μM for 6 h) (25),

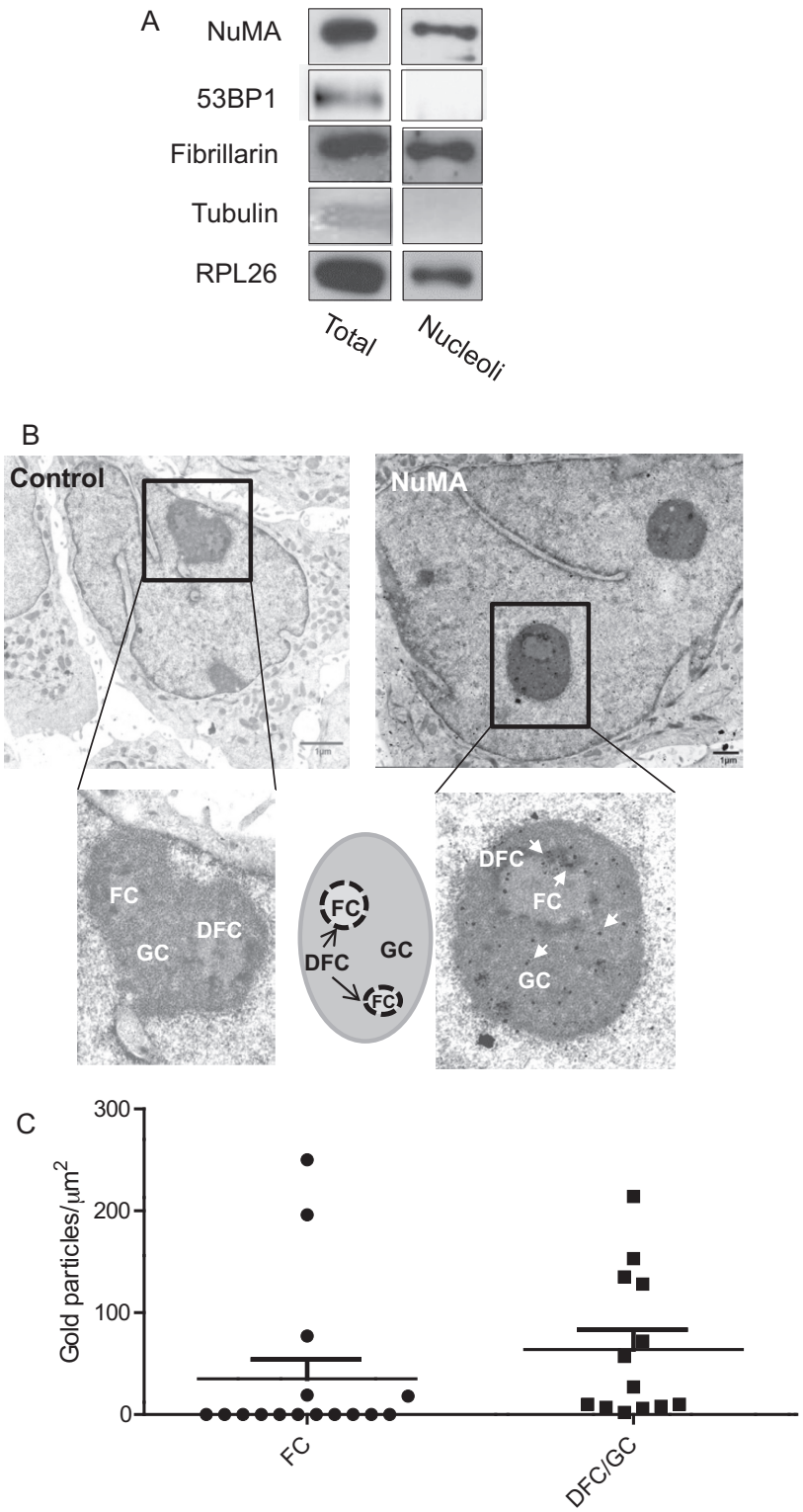

Figure 1. NuMA is present in the nucleolus of mammary epithelial cells. (**A**) Immunoblots for NuMA, ribosome-associated proteins fibrillarin and RPL26, cytoplasmic marker α-Tubulin and nucleoplasmic 53BP1 in total protein extracts (Total) and purified nucleoli fraction (Nucleoli) of T4–2 cells. (**B**). Electron micrographs of growth-arrested S1 cells (day 10) incubated with non-specific immunoglobulins (control) or with NuMA antibodies (NuMA) revealing the localization of NuMA (some of the gold particles [black dots] are indicated by arrows in the inset). A drawing illustrates the different nucleolar subcompartments. (**C**) Quantification of the distribution of NuMA gold immunolabeling particles within the FC and DFC/GC regions of the nucleoli as determined by the number of NuMA gold particles measured per area of FC and DFC/GC regions from the electron micrographs. The error bars on the scattered plot represent standard deviation. A total of eight nucleoli [areas ranging from ∼0.15 to 1 μm^2] were analyzed with four nuclei containing one nucleolus per nucleus, three nuclei containing two nucleoli per nucleus and one nucleus containing three nucleoli; FC, fibrillar center; DFC, dense fibrillar center; GC, granular center.

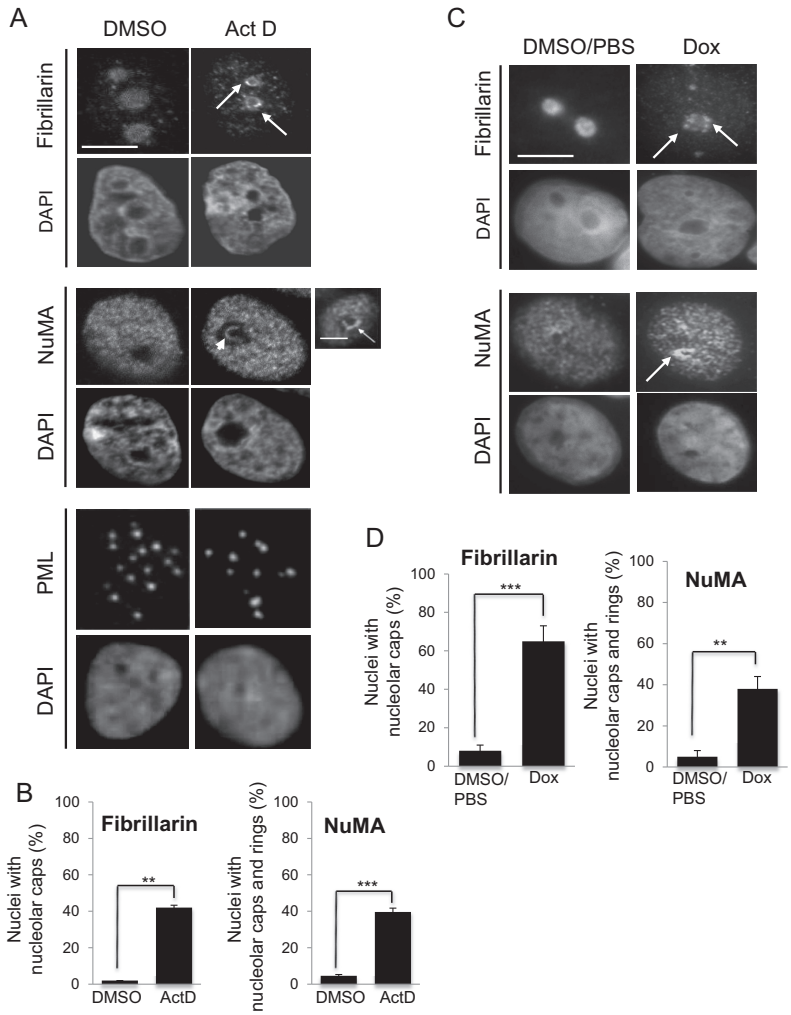

Figure 2. Inhibition of rDNA transcription by actinomycin D affects the distribution of NuMA. Growth-arrested S1 cells (10-day culture) treated with vehicle (DMSO) or 0.08 μg/ml of actinomycin D (Act D) for 4 h or treated with vehicle (DMSO/PBS) or 0.3 μM of doxorubicin (Dox) for 6 h at 37°C and immunostained for fibrillarin, NuMA and PML. The DNA is stained with DAPI. (**A** and **C**) The formation of the perinucleolar caps (arrows) and/or intranucleolar rings (arrowhead) upon actinomycin D (A) or doxorubicin (C) treatment is indicated. Scale bar: 5 μm. (**B** and **D**) Bar graphs of the percentages of intranucleolar and/or perinucleolar accumulation for fibrillarin and NuMA. $^{**}P < 0.01$, $^{***}P < 0.001$; unpaired Student's *t*-test. [Total number of nuclei scored per replicate: >300, $n = 3$; note: three technical replicates for Dox].

induced fibrillarin perinuclear caps as expected and also the perinucleolar redistribution of NuMA, whereas vehicle treatment (DMSO/PBS 1:1) did not induce such patterns (Figure 2C and D). Interestingly, the perinucleolar accumulation of NuMA and fibrillarin was strongly observed in non-proliferating cells; this phenomenon was also detected, but often less strikingly in proliferating cells (Supplementary Figure S2). Hence, NuMA reacts to the direct inhibition of rDNA transcription, including in non-proliferating cells.

NuMA interacts with components of ribosomal biogenesis

In light of the presence of NuMA in the nucleolus, particularly in DFCs and GCs, in which ribosomal transcription and pre-assembly steps occur, we sought to determine whether this protein might be associated with the machinery and products of the ribosome factory. Our earlier findings of an interaction between NuMA and the members of the WICH complex, SNF2h and WSTF (12) prompted us to investigate whether NuMA also interacted with NM1, which along with SNF2h and WSTF, forms the B-WICH complex involved in active rDNA transcription (45). Immunoprecipitation experiments performed on nuclear fractions of non-neoplastic cells and cancer cells with either an antibody against the coiled-coil domain of NuMA (referred to as NuMA-CC) or non-specific IgG revealed the presence of NM1, the third member of the B-WICH complex, in the NuMA-CC antibody precipitate (Figure 3A and Supplementary Figure S3A). In addition, NuMA antibodies also precipitated RNA polymerase I (Figure 3B and Supplementary Figure S3B) that mediates rDNA transcription and is known to interact with NM1 (46).

The presence of NuMA in the nucleolus and its interaction with proteins involved in chromatin remodeling and transcription in the nucleolus, suggested that NuMA might be located at rDNA genes. Indeed, ChIP revealed the pres-

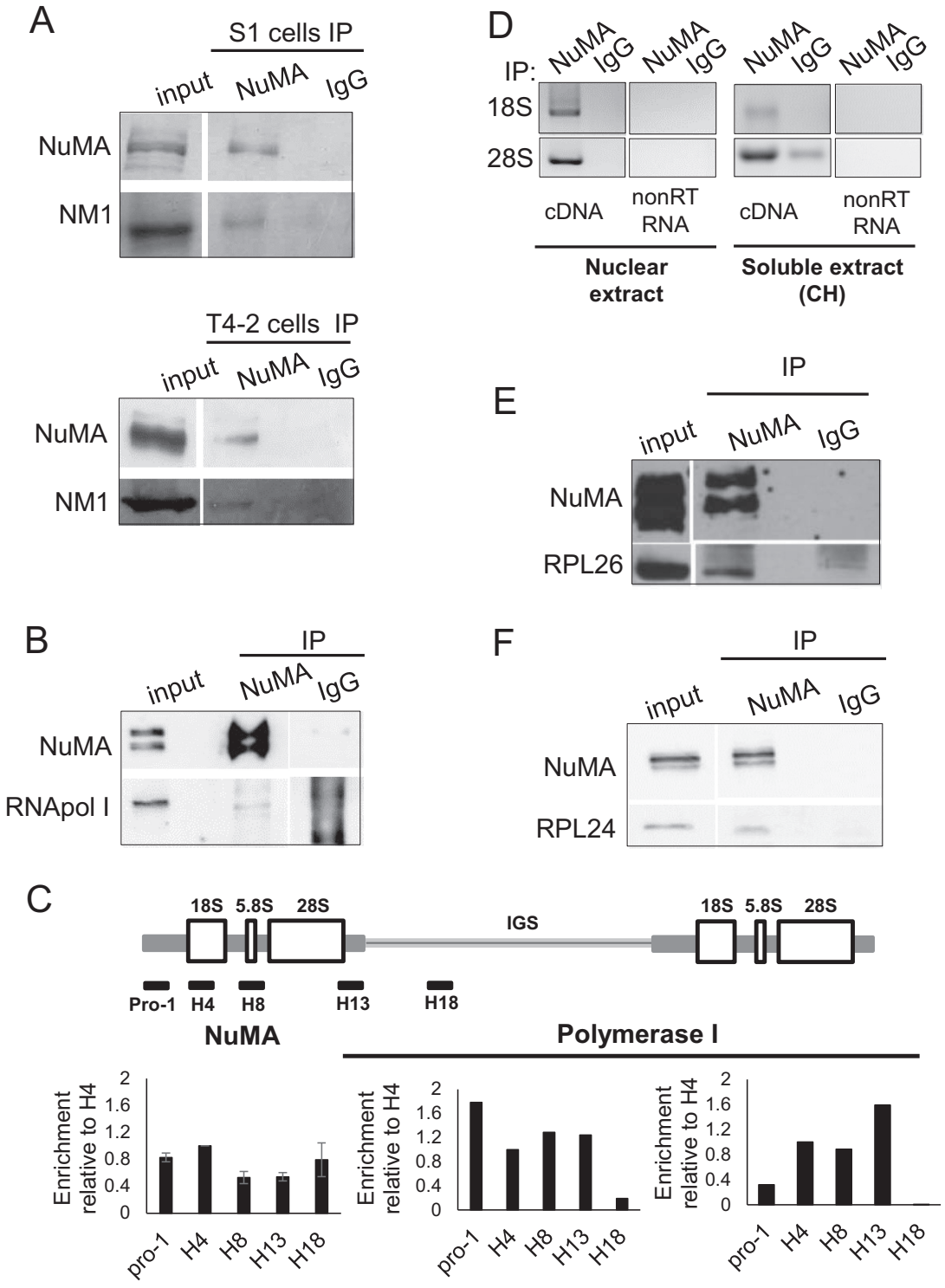

Figure 3. NuMA interacts with proteins and nucleic acid components of ribosomal biogenesis. S1 cells were cultured for 8 days with complete medium followed by 2 days without EGF to induce proliferation arrest; T4–2 cells were cultured for 6 days. (**A**) Immunoprecipitation (IP) of nuclear extracts from S1 and T4–2 cells with NuMA antibodies (NuMA) or with non-specific immunoglobulins (IgG), followed by western blot analysis of the input and immunoprecipitated samples using NuMA and NM1 antibodies. (**B**) Immunoprecipitation of nuclear extracts from S1 cells followed by western blot analysis for NuMA and RNA polymerase I (RNA pol I). (**C**) ChIP from T4–2 cells with NuMA antibody ($n = 4$) or RNA Polymerase I antibody ($n = 2$), followed by RT-qPCR for coding (pro-1, H4, H8, H13) and non-coding (H18) regions of rDNA. The drawing shows the organization of the rDNA gene (IGS = intergenic sequence). Data are normalized to those obtained with IgG control (see 'Materials and Methods' section). (**D**) RNA immunoprecipitation fromT4–2 cells with NuMA antibody or with non-specific IgG of nuclear extracts and soluble extracts (the latter were treated with 50 μg/ml cycloheximide [CH]). Both the DNAse treated non-reverse transcribed RNA (nonRT RNA) and the DNAse treated reverse-transcribed cDNA (cDNA) samples were subjected to PCR using primers specific for human 18S and 28S rRNAs ($n = 2$). (**E** and **F**) Immunoprecipitation of nuclear extracts from S1 cells followed by western blot analysis for NuMA, RPL26 and RPL24.

ence of NuMA at the rDNA promoter and gene body regions when compared to positive control, RNA Polymerase I (Figure 3C); the NuMA binding pattern was lost with ChIP performed with T4–2 cells with decreased NuMA expression induced by transfecting siRNA against NuMA (Supplementary Figure S4). Since rDNA transcription is intimately associated with the first step of rRNA processing, i.e. the production of the 45S rRNA transcript, and its splicing into 28S, 5.8S rRNAs and 18S rRNAs in the DFC region, we also investigated the potential interaction of NuMA with these rRNAs. Bioinformatics tools BindN (30) and RNABindR (31) provide algorithms to predict the presence of putative RNA-interacting residues in proteins with unknown structures. Computational analysis of the full-length NuMA protein sequence identified, with both tools, a 12-amino acid region (residues 2064–2075) spanning the C-terminus (CT) of NuMA as potential RNA-interacting domain (Supplementary Figure S5). In agreement with these predictions, RNA immunoprecipitation with NuMA-CC antibody, but not IgG, confirmed interactions between NuMA and the large subunit-associated 28S rRNA as well as the small subunit-associated 18S rRNA in nuclear extracts, and also in soluble extracts that were treated with cyclohexamide to prevent potential interaction linked to NuMA translation (Figure 3D and Supplementary Figure S3C). While NuMA-CC antibodies immunoprecipitated 45S rRNA, the presence of 45S rRNA in the IgG antibody pull-down fraction made the interpretation of NuMA interaction with 45S rRNA inconclusive (data not shown).

The abundance of NuMA in the DFC/GC regions of the nucleolus, where early and late stages of rRNA processing occur, and the binding of NuMA to rRNAs called for the investigation of NuMA interaction with ribosomal proteins. Immunoprecipitation of nuclear extracts with NuMA-CC antibody brought down ribosomal proteins RPL26 and RPL24 (Figure 3E and F; Supplementary Figure S3D and E). Incidentally, we have also identified RPL24 as a potential interacting partner in a mass spectrometry analysis of NuMA immunoprecipitation from HeLa nuclear extracts with two different NuMA antibodies (unpublished data). While NuMA's breadth of interaction with elements of ribosome biogenesis (rDNA, rRNAs and ribosomal proteins) suggests an overall role in this central nucleolar function, such level of interaction is akin to the nucleolar protein nucleolin that interacts with various elements of ribosome biogenesis and participates in multiple steps of this process (47–49), and the depletion of which results in altered events associated with nucleolar stress response, notably reduced nascent and pre-rRNA levels and cell cycle arrest (50).

Silencing NuMA decreases rRNA levels and triggers a p53-independent nucleolar stress response

Given the association of NuMA with processes that are linked to cellular homeostasis, the functional involvement of NuMA in nucleolar stress was further investigated. The interaction of NuMA with rDNA transcription components, i.e. rDNA, RNA polymerase I and B-WICH members, suggested that NuMA may influence the transcription step of ribosome biogenesis. Indeed, silencing of NuMA with siRNAs led to a decrease in the levels of 45S, 28S and 18S rRNAs in all replicates (Figure 4A) as well as nascent rRNAs, as shown by the loss of FUrd staining (Figure 4B). The reduction in the amount of NuMA did not affect the expression levels of RNA polymerase I and B-WICH complex members SNF2h, WSTF and NM1 compared to non-targeting siRNA control cells (Figure 4C). There was no statistically significant change either in the amounts of ribosome-associated protein RPS3 or those, including RPL26 and RPL24, for which an increase has been associated with p53-dependent nucleolar stress. Yet, the amount of RPL26 showed a tendency to increase in the three biological replicates (Figure 4C). RPL26 increase has been linked to p53 upregulation (51), and an increase in p53 amount has been associated with p53-dependent nucleolar stress response. Moreover, ectopic expression of NuMA in HeLa cells was shown to enhance the expression of p53 and p53 downstream genes, thereby linking NuMA to p53 regulation (15). Here, we observed that NuMA silencing did not significantly affect p53 levels in the S1 cell population, in which at least 50% of the cells usually express wild-type (WT)-p53 (Figure 4C and Supplementary Figure S6A). These cells are predominantly not proliferating by the peak time for NuMA silencing (6 days post-transfection) and when we collect the cells for analysis. Proliferating MCF7 breast cancer cells that contain WT-p53 (http://p53.iarc.fr/celllines.aspx) showed an increase in p53 levels upon silencing NuMA under proliferative conditions, but not under non-proliferative conditions, in the absence of serum; while RPL26 expression was not affected (Supplementary Figure S6B). Moreover, there was no apparent impact on the distribution of the stress sensor B23 (data not shown), ruling out a p53-dependent nucleolar stress response caused by NuMA downregulation. Hence, there might be a differential effect of NuMA silencing on p53 level depending on the cell cycle status that is independent from a nucleolar stress response.

Nucleolar stress has been divided into p53-dependent and p53-independent pathways (17,52). The p53-dependent nucleolar stress response is characterized by an increase in p53, which we do not observe upon NuMA silencing. To further investigate whether NuMA silencing leading to decreased rRNA levels might be associated with nucleolar stress we assessed additional-specific morphological and protein expression parameters of p53-dependent and p53-independent pathways. The lack of p53-dependent nucleolar stress response upon NuMA silencing was further supported by the absence of relocation of C23 (nucleolin) and B23 (nucleophosmin) from the nucleolus to the nucleoplasm (Supplementary Figure S7A and B). However, silencing NuMA led to the relocation of fibrillarin to the periphery of the nucleolus, which is a morphological sign of nucleolar stress (Figure 5A and B). Western blot analysis for $p27^{kip1}$, a marker of p53-independent nucleolar stress pathway revealed that silencing NuMA increased $p27^{kip1}$ expression (Figure 5C), and analysis of p53 expression overall confirmed no significant increase in these experiments (Figure 5D). Nucleolar stress induced by actinomycin D that leads to the formation of NuMA perinucleolar rings described above (Figure 2) was also accompanied with an increase in $p27^{kip1}$ expression, along with the formation of perin-

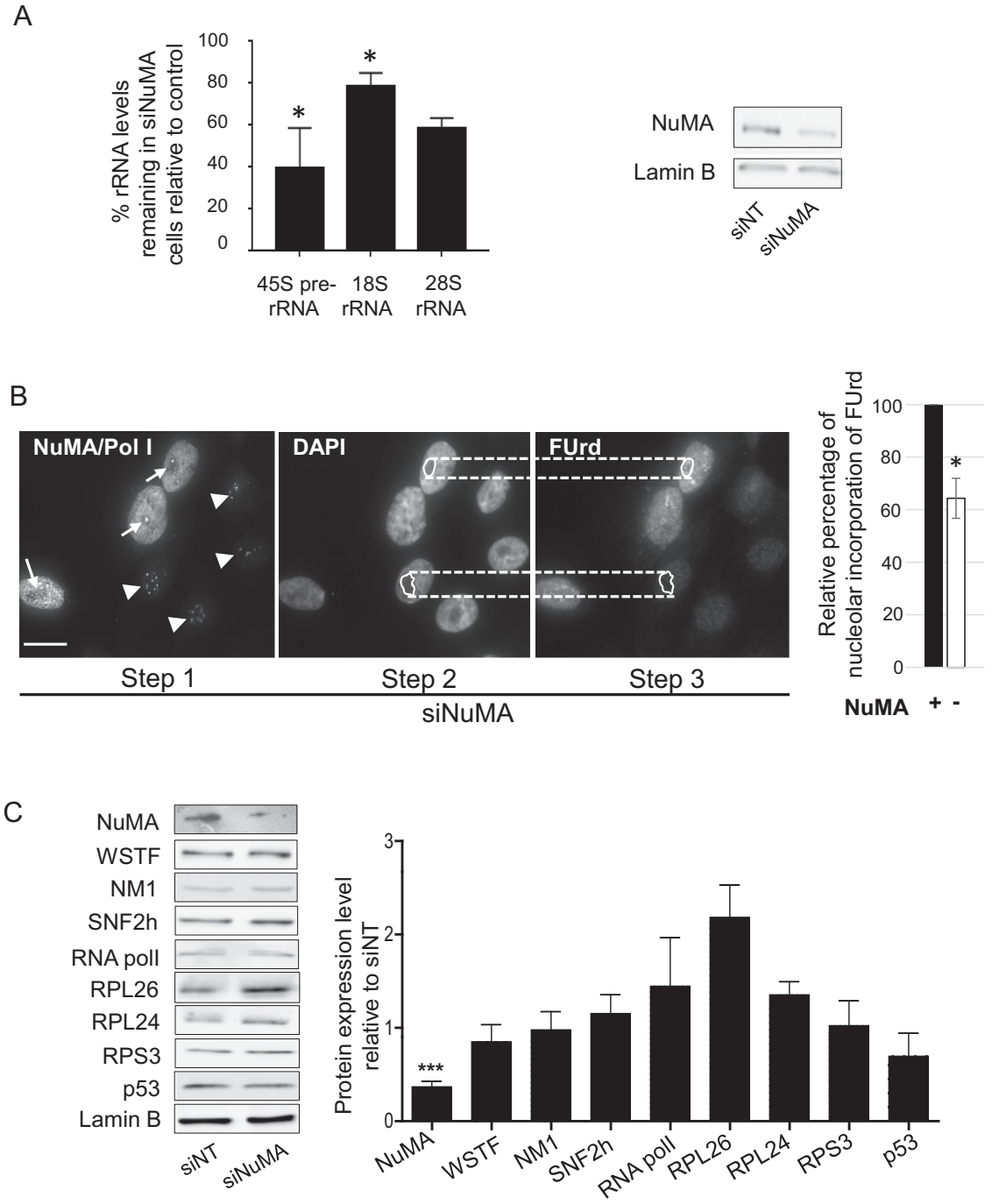

Figure 4. Silencing NuMA reduces rRNA levels with no significant impact on proteins associated with ribosomal biogenesis or p53-dependent nucleolar stress response. S1 cells were transfected with siRNA for NuMA (siNuMA) or non-targeting sequence (siNT) and left in culture until day 8. (**A**) Quantitative RT-PCR for 45S prerRNA, and related 18S RNA and 28S RNA. Representative western blot of the decrease in NuMA expression upon siRNA treatment is shown. Lamin B is used as loading control. (**B**) FUrd labeled nascent rRNA in siNuMA treated cells. Analysis was done by triple immunostaining for NuMA, Polymerase I [Pol I] and FUrd. The unique location of Pol I in the nucleolus (Step 1) was used to confirm that the weaker areas on DAPI stained nuclei are indeed nucleoli (Step 2). Upon delineating the nucleolar area on DAPI images, this area was then used for corresponding FUrd stained nuclei (Step 3) to perform the analysis as indicated in the 'Materials and Methods' section. Cells silenced for NuMA are revealed by the absence of immunostaining in the nucleoplasm (see nuclei with arrowhead indicating Pol I staining; nuclei that still show NuMA staining include an arrow to indicate Pol I staining). Bar graph shows the relative intensity of FUrd staining in the nucleoli of cells with (+) or without (−) NuMA expression. Over 30 cells were analyzed for each treatment condition ($n = 3$). (**C**) Protein quantification by western blot analysis in cells treated with siNuMA relative to levels in siNT-treated cells. Shown are representative western blot images. Lamin B is used as loading control. Size bar, 10 μm; $^{*}P < 0.05$, $^{***}P < 0{,}001$; one sample *t*-test.

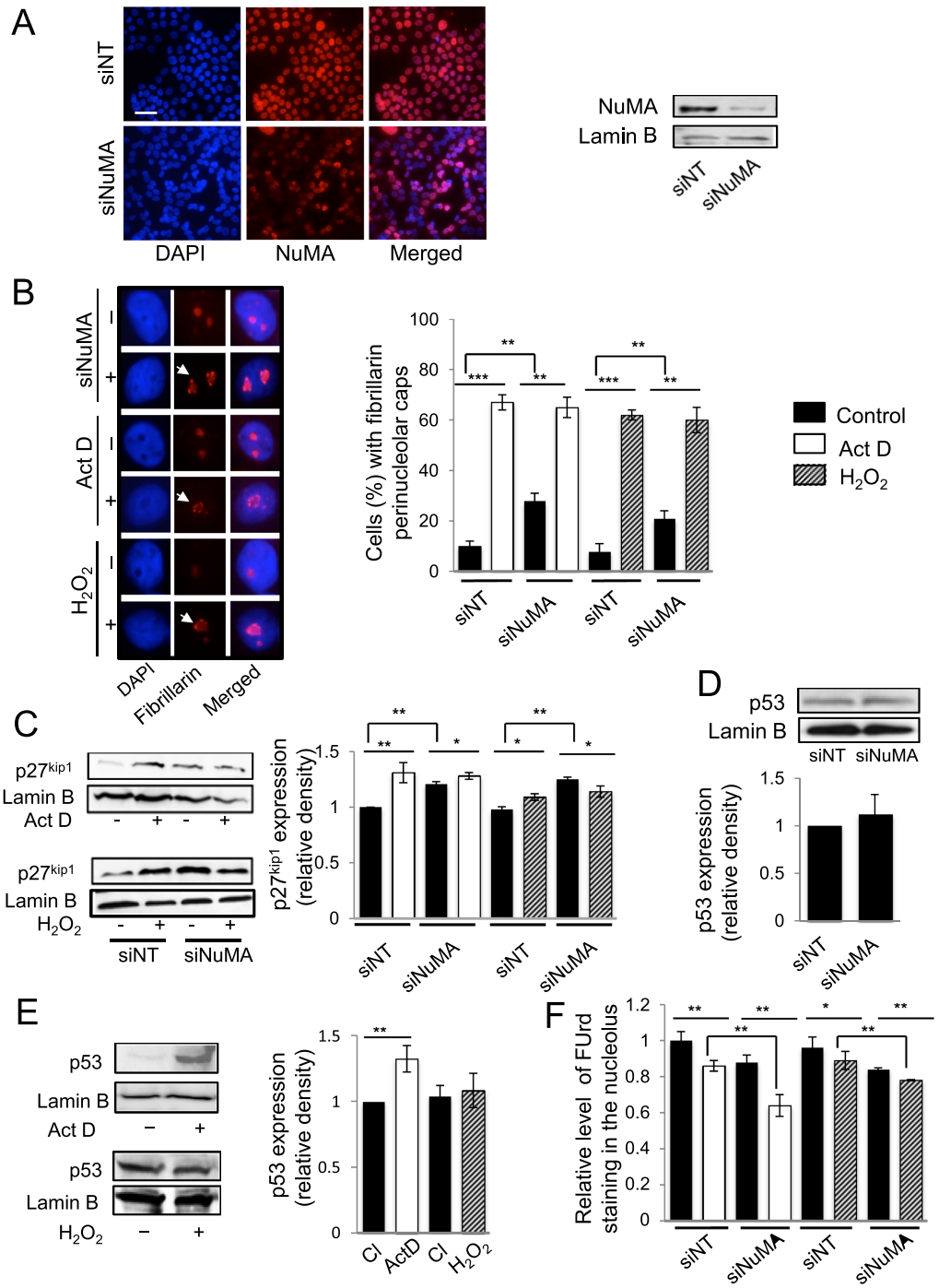

Figure 5. Silencing NuMA and treatment with ROS leads to p53-independent nucleolar stress response. S1 cells were treated with either siRNAs against NuMA (siNuMA) or non-targeting siRNA (siNT) and left in culture for 10 days, and/or with 0.08 μg/ml actinomycin D (Act D) or control DMSO for 4 h on day 10, and/or with 250 μM of H_2O_2 for 4 h on day 10. (**A**) Immunostaining for NuMA (red) with nuclei stained with DAPI (blue). Also shown is a representative western blot for NuMA; lamin B is used as loading control. (**B**) Representative images of nuclei stained in red for fibrillarin. Note their nucleolar distribution in the 'control' (−) cultures. Arrows indicate the formation of perinucleolar caps of fibrillarin in all treatments. Nuclei are stained with DAPI (blue). The bar graph shows the percentage of cells with perinucleolar caps of fibrillarin indicative of nucleolar stress ($n = 3$; 150 nuclei analyzed per condition). (**C**) Western blot for $p27^{kip1}$, following Act D or H_2O_2 treatment in the presence (siNuMA) or absence (siNT) of siRNA against NuMA; lamin B is used as loading control. The graph shows $p27^{kip1}$ levels under the different conditions relative to siNT control after standardization against lamin B ($n = 3$). (**D**) Bar graph of p53 expression following quantification by western blot analysis in cells treated with siNT or with siNuMA for the same replicates as in E and relative to siNT; ($n = 3$); shown is a representative western blot image. (**E**) Representative western blots for p53 with lamin B used as loading control in cells treated with Act D or H_2O_2. The bar graph shows p53 quantification ($n = 3$). (**F**) Levels of FUrd staining for nascent rRNA (nucleolus) following normalization to nucleoplasmic staining intensity (nascent mRNAs) under the different treatment conditions ($n = 3$; 100 nuclei analyzed per condition). $^*P < 0.05$; $^{**}P < 0.01$; $^{***}P < 0.001$; one sample *t*-test [A, D, E] and multiple-factor ANOVA Tukey's post hoc test [B, C, F]; *note*: for C and F, individual comparison to the first siNT that is standardized on the graph was done with one sample *t*-test. Size bar, 50 μm.

ucleolar caps of fibrillarin. However, p53 was also found to be upregulated upon actinomycin D treatment, corroborating B23 and C23 redistribution, and indicating that both p53-dependent and p53-independent nucleolar stress response pathways are functionally active in S1 cells (Figure 5E and Supplementary Figure S7B). Doxorubicin treatment recapitulated the effect of actinomycin D on fibrillarin perinucleoar cap or ring formation and C23 and B23 relocation and p53 increase (Figure 2 and Supplementary Figure S7C). Actinomycin D or doxorubcin treatment of siNuMA-transfected S1 cells led to further increase in the number of cells showing fibrillarin perinucleolar caps compared to siNuMA cells (Figure 5B; Supplementary Figure S7D and E); similarly, the reduction in ribosomal nascent RNA level measured by FUrd staining was significantly enhanced upon actinomycin D or doxorubicin treatment of siNuMA cells compared to siNuMA cells treated with vehicle. Conversely, significant additive impact of NuMA silencing on actinomycin D or doxorubicin treatment was measured on nascent RNA formation, reinforcing the strong impact of NuMA on rDNA transcription (Figure 5F and Supplementary Figure S7F). To confirm results with S1 cells we repeated experiments with another non-neoplastic mammary epithelial cell line, MCF10A, that contains WT-p53 (53). These cells behaved similarly to S1 cells with regards to fibrillarin perinucleolar cap formation, B23 and C23 localization, and FUrd and $p27^{kip1}$ levels in the presence of actinomycin D with or without NuMA silencing (Figure 6A, B and E; Supplementary Figure S8A–C). Like with S1 cells, C23 relocalization upon actinomycin D treatment in MCF10A cells was accompanied with an increase in p53 levels (Supplementary Figure S8D). To strengthen the possibility for NuMA to control nucleolar stress in the absence of p53, MDA-MB-157 cells that are depleted for this protein (23) were silenced for NuMA. Loss of NuMA was accompanied with the formation of perinucleolar caps of fibrillarin and reduced FUrd levels (Figure 6C and D; Supplementary Figure S8A and C). Surprisingly, no significant $p27^{kip1}$ increase was observed (Figure 6F and Supplementary Figure S8B). When cells were treated with actinomycin D they showed nucleolar stress based on B23 relocalization, fibrillarin perinucleolar cap formation and decrease in FUrd labeling, indicating a stress response (Figure 6 and Supplementary Figure S8). Yet, there was still no significant increase in $p27^{kip1}$ (Figure 6F and Supplementary Figure S8B). In fact, these cells displayed higher amounts of $p27^{kip1}$ and lower amounts of NuMA compared to S1 and MCF10A cells already in the absence of induction of nucleolar stress (Figure 6G), suggesting the possibility of an intrinsic $p27^{kip1}$ elevation in cells exhibiting reduced NuMA expression.

Actinomycin D and doxorubicin treatments induce nucleolar stress in a pharmacological or non-natural manner, whereas the activity of ROS is a physiologically relevant inducer of nucleolar stress. Upon treatment of S1 cells with 250 μM of H_2O_2 for 4 h, fibrillarin formed perinucleolar caps, B23 redistributed but not C23 and nascent RNA levels were decreased. Western blot confirmed an increase in $p27^{kip1}$ expression, but no change in p53 expression, illustrating a p53-independent pathway for ROS-mediated nucleolar stress response. Like with actinomycin D and doxorubicin, NuMA silencing with ROS treatment further amplified the decrease in nascent rRNA levels (Figure 5B, C, E and F and Supplementary Figure S7B). Treatment with ROS also induced nucleolar stress in MCF10A cells and in MDA-MB157 cells, based on the formation of fibrillarin perinucleolar caps, B23 relocation and a decrease in FUrd labeling (Figure 6 and Supplementary Figure S8). In contrast to S1 cells, MCF10A cells showed relocation of C23 upon H_2O_2 treatment (Supplementary Figure S8C). Accordingly, an increase in p53 levels was also recorded in these cells (Supplementary Figure S8D). Importantly, the additional reduction of nascent rRNA amount upon ROS or actinomycin D treatment of siNuMA-cells compared to untreated cells (Figure 5F) was accompanied by further reduction in NuMA levels measured by immunofluorescence and western blot analysis (Figure 7A and B). Independent experiments showed that in S1 cells differentiated into acini representing phenotypically normal differentiation, ROS treatment leading to oxidative stress response, as measured by AOP2 induction, indeed decreased NuMA level (Figure 7C). These data suggest that a NuMA-based mechanism is involved in the physiologically relevant induction of nucleolar stress with ROS.

DISCUSSION

In this study, contrary to the widely accepted notion that NuMA is excluded from the nucleolus of interphase nuclei based on immunofluorescence studies (20,54,55) we provide evidence that NuMA is present in the nucleolus of both non-neoplastic and cancerous mammary epithelial cells. This finding corroborates the description of the nucleolar proteome in HeLa cells that identified NuMA as a potential nucleolar protein (18,19). We further provide evidence that NuMA participates in rDNA transcription, and that attenuating NuMA expression induces a p53-independent nucleolar stress response. One of the mechanisms by which proteins enter the nucleolus is through the presence of nucleolar targeting signals (e.g. RNA-binding domains, NoLS) in their sequence. The presence of a putative NoLS signal in the CT domain of NuMA warrants further investigation to clarify the entry of NuMA into the nucleolus.

NuMA is known to influence chromatin organization, to regulate p53-dependent gene transcription and to interact with transcription-associated proteins (1,12,14,56,57). All of these activities implicate NuMA in the regulation of gene transcription. Here, we show that NuMA participates in rDNA transcription based on its interaction with RNA polymerase I and B-WICH proteins that are members of the rDNA transcription initiation machinery, and its recruitment to rDNA promoter region. This possibility is reinforced by the observation that NuMA silencing leads to reduced levels of nascent pre-rRNA, directly produced from rDNA transcription, and to the formation of fibrillarin perinucleolar caps, a nucleolar stress response behavior linked to inhibition of rDNA transcription. The reduced levels of rRNAs that are by-products of nascent pre-rRNA processing, are likely secondary effects of reduced pre-rRNA levels. NuMA lacks DNA-binding motifs or enzymatic activity and is considered as a scaffold protein, owing to the presence of an unusually long coiled-coil domain

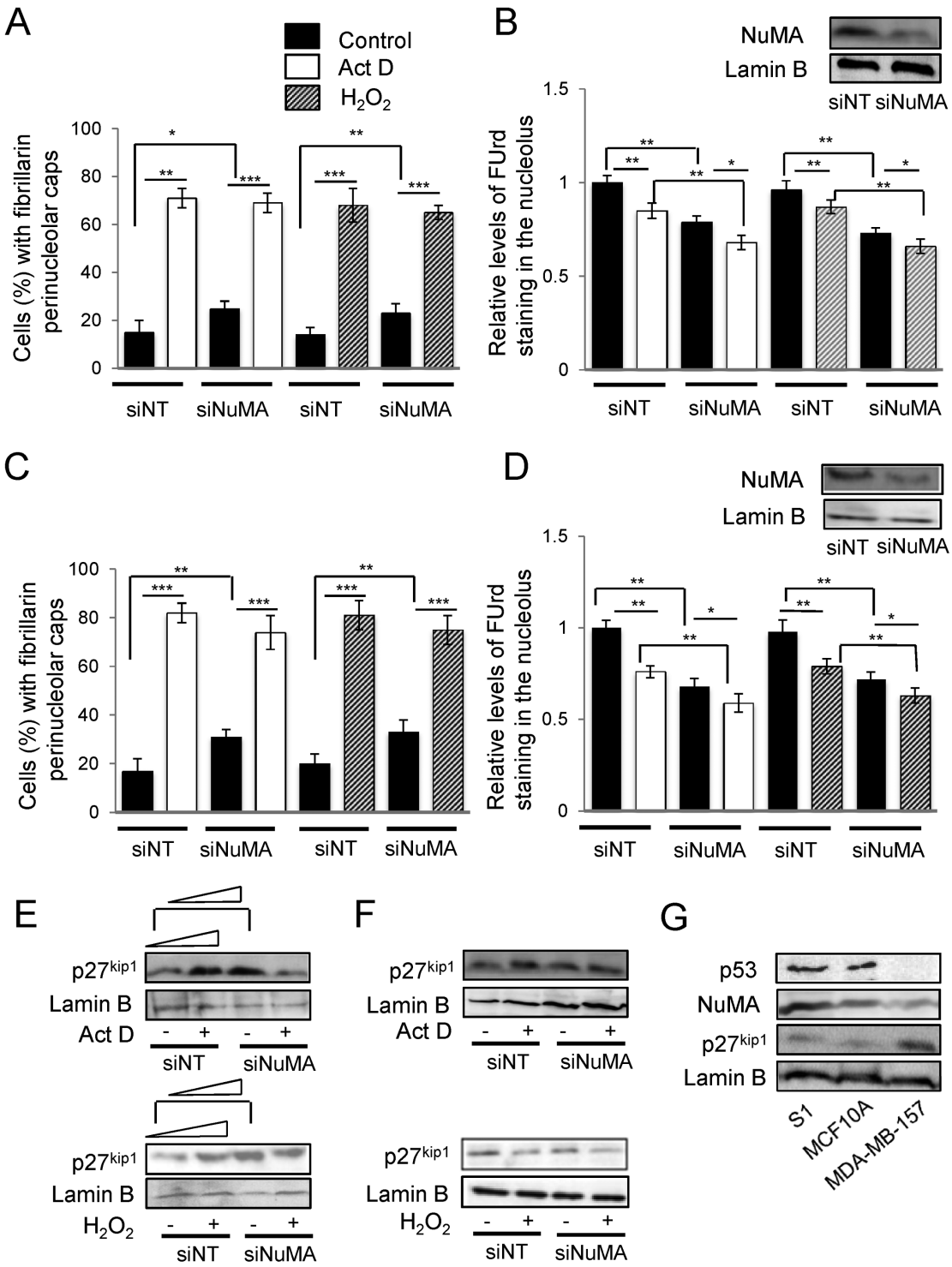

Figure 6. Silencing NuMA and treatments with actinomycin D and H_2O_2 lead to $p27^{kip1}$ increase unless it is already elevated. MCF10A WT-p53 cells and p53-null MDA-MB-157 cells were treated with either siRNA against NuMA (siNuMA) or non-targeting siRNA (siNT) and left in culture for 10 (MCF10A) or eight (MDA-MB-157) days, and/or with 0.08 μg/ml actinomycin D (Act D) or control DMSO for 4 h on day 10 (or 8), and/or with 250 μM of H_2O_2 for 4 h on day 10 (or 8). (**A** and **C**). Percentage of cells with perinucleolar caps of fibrillarin indicative of nucleolar stress ($n = 3$; 150 nuclei analyzed per condition) in MCF10A (A) and MDA-MB-157 (C) populations. (**B** and **D**). Levels of FUrd staining for nascent rRNA (nucleolus) following normalization to nucleoplasmic staining intensity (nascent mRNAs) under the different treatment conditions ($n = 3$; 100 nuclei analyzed per condition). Shown is a representative western blot of NuMA expression upon siNuMA treatment in MCF10A cells (B) and MDA-MB-157 cells (D). (**E** and **F**). Western blot and accompanying quantification (following standardization with lamin B and compared to the first band of each western blot) for $p27^{kip1}$, following Act D or H_2O_2 treatment in the presence (siNuMA) or absence (siNT) of siRNA against NuMA; lamin B is used as loading control in MCF10A (E) and MDA-MB-157 (F) cells. (**G**). Western blot for p53, NuMA, $p27^{kip1}$ and loading control lamin B in untreated S1, MCF10A and MDA-MB-157 cells.

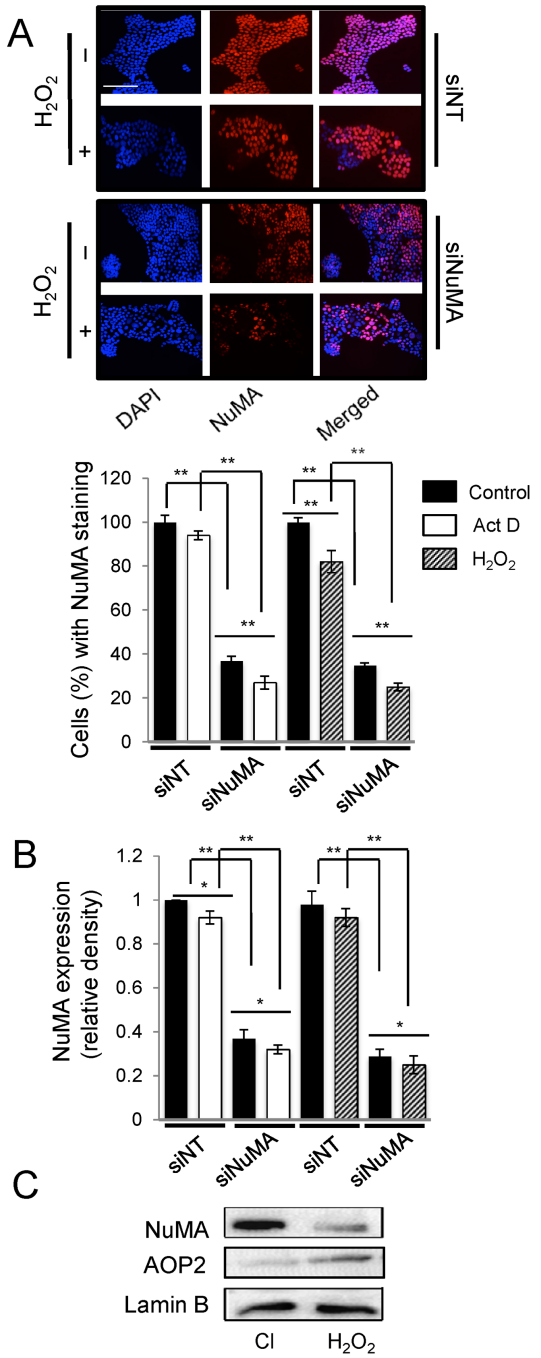

Figure 7. Treatments with Actinomycin D and H_2O_2 decrease NuMA expression. S1 cells were treated with either siRNAs against NuMA (siNuMA) or non-targeting siRNA (siNT) and left in culture for 10 days before incubation with 250 μM of H_2O_2 or with 0.08 μg/ml actinomycin D (Act. D) for 4 h on day 10. (**A**). Immunostaining for NuMA (red); nuclei are stained with DAPI (blue) following H_2O_2 treatment. The bar graph shows the percentage of cells with NuMA staining under all treatment conditions ($n = 3$; 150 nuclei analyzed per condition). (**B**) Bar graph of NuMA quantification following western blots and standardization to loading control lamin B under all treatment conditions. (**C**) Representative western blots for NuMA, oxidative stress response marker AOP2 and loading control lamin B following treatment of S1 cells differentiated into acini in 3D culture with 250 μM of H_2O_2 for 4 h (Cl = vehicle control). $^*P < 0.05$; $^{**}P < 0.01$; multiple-factor ANOVA and Tukey's posthoc test; *note*: for B, individual comparison to the first siNT that is standardized on the graph was done with one sample *t*-test. Size bar, 100 μm.

in its sequence (58). Reports have proposed a scaffold function for NuMA in facilitating the assembly of the mediator complex during p53-mediated gene transcription (14) and in orchestrating the initial chromatin events of the DNA repair response (12). Therefore, we postulate that NuMA may exert a similar function in rDNA transcription, wherein it might orchestrate the interaction of proteins associated with the rDNA transcription initiation complex (e.g. RNA pol I, B-WICH, co-factors) at the rDNA promoter region and facilitate the initiation of rDNA transcription. Whether currently known protein partners of NuMA, in addition to SNF2h (12) and RNA polymerase I, might be involved in the regulation of rDNA transcription remains to be established; the influence of NuMA on B-WICH and polymerase I appears like a good starting point for further investigations of NuMA-mediated control mechanisms. Intriguingly, NuMA shows a slightly different rDNA binding pattern compared to Polymerase I, with a peak in binding for H18 that is part of the intergenic region, whereas as expected, polymerase I does not bind this region. This observation calls for further analysis of a possible link with an anchorage role for the nuclear matrix portion of NuMA (8), as previously suggested along the DNA matrix attachment regions (59).

The binding of NuMA to a number of very different proteins, and its involvement in multiple major cellular functions (from mitotic spindle maintenance to several nuclear pathways for gene expression and DNA repair control) brings the issue of the regulation of these interactions. A number of reports have now demonstrated posttranslational modifications for NuMA, such as phosphorylation (60–66), glycosylation (67), sumoylation (68) and ubiquitination (69), some of which might account for the changing patterns of NuMA bands seen by electrophoresis (e.g. NuMA often appears as a doublet, as shown on several of our western blot images). The majority of the work on posttranslational modifications for NuMA has been performed in the context of mitosis (although we showed phosphorylation in the context DNA repair as well (12)). Hence, thorough experimental and computational analyses of the consequences of each post-translational modification on the interaction between NuMA and proteins or nucleic acids will help integrate the different locations, functions and binding partners of NuMA into a comprehensive map. These analyses appear particularly important because NuMA might be working not only in several compartments in the cell nucleus, but also in the cytoplasm like we have observed in S1 cells (unpublished data), which raises the question of whether its link with the soluble fraction containing rRNAs that we show in this report might represent cytoplasmic interaction as well.

The nucleolus responds to various stress signals in either a p53-dependent or p53-independent manner (17,52). While the mechanism of p53-independent nucleolar stress response remains to be fully understood, reports indicate that ribosomal proteins such as RPL3 might be involved in mediating part of the cellular response to nucleolar stress in certain cells lacking functional p53 or upon exposure to DNA damaging agents other than actinomycin D in $p53^{-/-}$ cells (70,71). However, induction of nucleolar stress has been associated with upregulation of $p27^{kip1}$ expression

in cell lines with either functional p53 or non-functional p53 (72,73), highlighting that $p27^{kip1}$ involvement in p53-independent mechanisms does not require the loss of p53. We have shown that the expression of both p53 and $p27^{kip1}$ (a p53-independent stress signal) is enhanced upon actinomycin D-induced inhibition of rDNA transcription in S1 cells, whereas expression of $p27^{kip1}$, but not p53 is enhanced upon inhibition of rDNA transcription by ROS treatment or NuMA silencing. One possible explanation for these different outcomes is that actinomycin D intercalates into the DNA, and may thereby directly and potently attenuate rDNA transcription by blocking polymerase I activity, and hence stimulate downstream nucleolar stress response signals including $p27^{kip1}$ and p53. This pharmacological approach to inhibit rDNA transcription is widely reported in the literature, yet it does not reflect rDNA transcription inhibition under physiological conditions. Instead, exposure of cells to environmental insults such as heat shock, acidosis and oxidative stress are physiologically relevant situations and, *in vitro* studies have confirmed that these stressors influence rDNA transcription (74–77). However, upon our literature search we could not find studies with these nucleolar stressors that have investigated in details the downstream nucleolar stress signals (p53 dependent and independent). Besides, other studies have shown that the aforementioned stressors can activate p53 expression *in vitro* (78–80), but the effect on rDNA transcription was not evaluated. Likewise, it was shown that oxidative stress induction by H_2O_2 treatment (100 μM for 12 h) in non-neoplastic and malignant cells suppresses $p27^{kip1}$ expression (81), but rDNA transcription status was not evaluated in this study. Clearly, there is a dearth of knowledge on the nucleolar stress response mechanisms that are activated under physiologically relevant stress conditions. In our study, we show that oxidative stress induction (250 μM H_2O_2 treatment for 4 h) enhances $p27^{kip1}$ expression in S1 and MCF10A cells, which is expected if this pathway is involved in the nucleolar stress response. It is possible that a different concentration of H_2O_2 and the extent of exposure might affect $p27^{kip1}$ expression differently, with extended oxidative stress induction having a tendency to reduce $p27^{kip1}$ expression. The protein $p27^{kip1}$ is a cell cycle inhibitor that plays an important role both in the process of cell differentiation (82–86) and in the maintenance of cells in G0/G1 arrested state (87,88). In response to ribosomal stress induced by RPS19 silencing, $p27^{kip1}$ expression has been reported to increase in both p53 expressing and p53 non-expressing human erythroleukemic cells, resulting in cell cycle arrest (73). Enhanced p53 expression was also observed upon RPS19 silencing in the p53 expressing cells. Given the well-established role of $p27^{kip1}$ in the maintenance of quiescence (89–91), it is plausible that the increased $p27^{kip1}$ expression in NuMA-silenced and ROS-treated growth-arrested S1 cells may play a role in maintaining the cells in a quiescent state. We also saw that, in contrast to S1 cells, MCF10A cells respond to ROS treatment by increasing p53 in addition to $p27^{kip1}$. This particular response might be a reflection of enhanced sensitivity of MCF10A cells to ROS action, notably its DNA damage induction or of the overall higher percentage of cells with WT-p53.

Interestingly, p53-independent nucleolar stress signal, but not p53 is activated in S1 cells in which NuMA is attenuated either directly (via silencing) or indirectly (via oxidative stress). It remains to be studied as to why $p27^{kip1}$ pathway, but not p53 is triggered upon NuMA reduction. Despite these cells partially expressing wild-type p53, it is possible that physiological inhibition of rDNA transcription involving NuMA may not require p53 activation. *In vitro* studies have shown that p53 levels are enhanced in cells sustaining DNA damage (92). Perhaps, the increase in p53 expression observed in actinomycin D-treated cells is a treatment-specific response triggered by drug induced-DNA damage. Under physiological conditions, the mechanism of rDNA inhibition is likely to be distinct from a drug-based approach. In any case, NuMA and p53 have a very different rapport to the nucleolus, since p53 has been reported to be in nucleolar cavities instead of the typical nucleolar regions associated with ribosomal biogenesis (93). The link between NuMA expression and $p27^{kip1}$ expression is further supported by the fact that, in our experiments, p53-depleted MDA-MB-157 breast cancer cells have lower NuMA level and higher $p27^{kip1}$ level than non-neoplastic S1 and MCF10A cells. Although MDA-MB-157 cells respond to nucleolar stress induced by actinomycin D and H_2O_2 treatments, they do not further increase $p27^{kip1}$, which might be linked to their status of low NuMA and already high $p27^{kip1}$, similar to what is observed in S1 and MCF10A cells in which NuMA expression has been experimentally decreased. How a decrease in NuMA expression affects $p27^{kip1}$ expression might be an interesting direction of study, especially in light of possible consequences for cancer outcomes as explained below.

NuMA has been functionally linked to several cellular processes including chromatin organization, gene transcription, DNA repair and apoptosis, all of which play a pivotal role in the maintenance of cellular homeostasis (1,7,8,11,12). The involvement of NuMA in rDNA transcription could be envisioned as an extended role in its homeostatic function, where upon exposure of non-neoplastic cells to environmental insults such as oxidative stress, the reduction of NuMA levels acts as a protective response to inhibit rDNA transcription. This notion is supported by reduced NuMA expression in differentiated S1 acini exposed to oxidative stress. Studies indicate that $p27^{kip1}$ expression is relatively high in normal breast tissues and non-malignant cell lines compared to breast cancer tissues and cell lines (94), with reduced $p27^{kip1}$ expression in multiple cancers, including breast cancer, inversely correlating with patient prognosis (95,96). Moreover, a number of studies support the fact that impaired ribosomal biogenesis can lead to cancer development, notably via the loss of mRNA translation to produce proteins with tumor suppressor activity (97–99), such as p53 and $p27^{kip1}$. We can envision a scenario in which sustained environmental stress like oxidative stress in non-malignant cells might decrease NuMA expression, hence inhibiting rDNA transcription and triggering nucleolar stress. The expression of $p27^{kip1}$ would initially increase in response to nucleolar stress, potentially maintaining the cells in a quiescent state. However, prolonged oxidative stress would attenuate $p27^{kip1}$ expression, possibly due to low ribosomal biogenesis. In support

of this idea, Zannoni *et al*. have shown that increased levels of intrinsic oxidative stress during malignant transformation of vulvar epithelial cells are associated with decreased $p27^{kip1}$ expression (100). An absence of p53 induction upon oxidative stress would further imbalance the cells toward cell cycle exit, with a lesser amount of NuMA preventing p53-targeted transcription of p21 (14). Thus, the reduced expression of NuMA and $p27^{kip1}$ induced by prolonged exposure to oxidative stress would not only enhance intrinsic cellular stress levels leading to stress resistance characteristic of cancer cells, but also facilitate cell cycle entry, ultimately driving malignant transformation.

SUPPLEMENTARY DATA

Supplementary Data are available at NAR Online.

ACKNOWLEDGEMENTS

We thank Jeffrey Nickerson for generously sharing NuMA B1C11 antibody.

FUNDING

National Cancer Institute, National Institutes of Health (NIH) [R01CA112017 to S.A.L., K99/R00CA163957 to P.A.V.]; Executive Vice President and Research Partnership Office at Purdue University (to S.A.L.); Purdue Center for Cancer Research NIH award [P30 CA023168]. Funding for open access charges: Purdue University Center for Cancer Research.
Conflict of interest statement. None declared.

REFERENCES

1. Abad,P.C., Lewis,J., Mian,I.S., Knowles,D.W., Sturgis,J., Badve,S., Xie,J. and Lelièvre,S.A. (2007) NuMA influences higher order chromatin organization in human mammary epithelium. *Mol. Biol. Cell*, **18**, 348–361.
2. Zeng,C., He,D. and Brinkley,B.R. (1994) Localization of NuMA protein isoforms in the nuclear matrix of mammalian cells. *Cell Motil. Cytoskeleton*, **29**, 167–176.
3. Lydersen,B.K. and Pettijohn,D.E. (1980) Human-specific nuclear protein that associates with the polar region of the mitotic apparatus: distribution in a human/hamster hybrid cell. *Cell*, **22**, 489–499.
4. Du,Q., Taylor,L., Compton,D.A. and Macara,I.G. (2002) LGN blocks the ability of NuMA to bind and stabilize microtubules. A mechanism for mitotic spindle assembly regulation. *Curr. Biol.*, **12**, 1928–1933.
5. Fant,X., Merdes,A. and Haren,L. (2004) Cell and molecular biology of spindle poles and NuMA. *Int. Rev. Cytol.*, **238**, 1–57.
6. Peyre,E., Jaouen,F., Saadaoui,M., Haren,L., Merdes,A., Durbec,P. and Morin,X. (2011) A lateral belt of cortical LGN and NuMA guides mitotic spindle movements and planar division in neuroepithelial cells.J. *Cell Biol.*, **193**, 141–154.
7. Chandramouly,G., Abad,P.C., Knowles,D.W. and Lelièvre,S.A. (2007) The control of tissue architecture over nuclear organization is crucial for epithelial cell fate. *J. Cell Sci.*, **120**, 1596–1606.
8. Lelièvre,S.A., Weaver,V.M., Nickerson,J.A., Larabell,C.A., Bhaumik,A., Petersen,O.W. and Bissell,M.J. (1998) Tissue phenotype depends on reciprocal interactions between the extracellular matrix and the structural organization of the nucleus. *Proc. Natl. Acad. Sci. U.S.A.*, **95**, 14711–14716.
9. Gribbon,C., Dahm,R., Prescott,A.R. and Quinlan,R.A. (2002) Association of the nuclear matrix component NuMA with the Cajal body and nuclear speckle compartments during transitions in transcriptional activity in lens cell differentiation. *Eur. J. Cell Biol.*, **81**, 557–566.
10. Barboro,P., D'Arrigo,C., Mormino,M., Coradeghini,R., Parodi,S., Patrone,E. and Balbi,C. (2003) An intranuclear frame for chromatin compartmentalization and higher-order folding. *J. Cell Biochem.*, **88**, 113–120.
11. Vidi,P.A., Chandramouly,G., Gray,M., Wang,L., Liu,E., Kim,J.J., Roukos,V., Bissell,M.J., Moghe,P.V. and Lelièvre,S.A. (2012) Interconnected contribution of tissue morphogenesis and the nuclear protein NuMA to the DNA damage response. *J. Cell Sci.*, **125**, 350–361.
12. Vidi,P.A, Liu,J., Salles,D., Jayaraman,S., Dorfman,G., Gray,M., Abad,P., Moghe,P.V., Irudayaraj,J.M., Wiesmüller,L. *et al.* (2014) NuMA promotes homologous recombination repair by regulating the accumulation of the ISWI ATPase SNF2h at DNA breaks. *Nucleic Acids Res.*, **42**, 6365–6379.
13. Lin,H.H., Hsu,H.L. and Yeh,N.H. (2007) Apoptotic cleavage of NuMA at the C-terminal end is related to nuclear disruption and death amplification. *J. Biomed. Sci.*, **14**, 681–694.
14. Ohata,H., Miyazaki,M., Otomo,R., Matsushima-Hibiya,Y., Otsubo,C., Nagase,T., Arakawa,H., Yokota,J., Nakagama,H., Taya,Y. *et al.* (2013) NuMA is required for the selective induction of p53 target genes. *Mol. Cell. Biol.,* **33**, 2447–2457.
15. Endo,A., Moyori,A., Kobayashi,A. and Wong,R.W. (2013) Nuclear mitotic apparatus protein, NuMA, modulates p53-mediated transcription in cancer cells. *Cell Death Dis.*, **4**, e713.
16. Grummt,I. (2013) The nucleolus—guardian of cellular homeostasis and genome integrity. *Chromosoma*, **122**, 487–497.
17. James,A., Wang,Y., Raje,H., Rosby,R. and DiMario,P. (2014) Nucleolar stress with and without p53. *Nucleus*, **5**, 402–426.
18. Andersen,J.S., Lyon,C.E., Fox,A.H., Leung,A.K., Lam,Y.W., Steen,H., Mann,M. and Lamond,A.I. (2002) Directed proteomic analysis of the human nucleolus. *Curr. Biol.*, **12**, 1–11.
19. Andersen,J.S., Lam,Y.W., Leung,A.K., Ong,S.E., Lyon,C.E., Lamond,A.I. and Mann,M. (2005) Nucleolar proteome dynamics. *Nature*, **433**, 77–83.
20. Compton,D.A. and Cleveland,D.W. (1993) NuMA is required for the proper completion of mitosis. *J. Cell Biol.*, **120**, 947–957.
21. Briand,P., Petersen,O.W. and Van Deurs,B. (1987) A new diploid nontumorigenic human breast epithelial cell line isolated and propagated in chemically defined medium. *In Vitro Cell Dev. Biol.*, **23**, 181–188.
22. Briand,P., Nielsen,K.V., Madsen,M.W. and Petersen,O.W. (1996) Trisomy 7p and malignant transformation of human breast epithelial cells following epidermal growth factor withdrawal. *Cancer Res.*, **56**, 2039–2044.
23. Bartek,J., Iggo,R., Gannon,J. and Lane,D.P. (1990) Genetic and immunochemical analysis of mutant p53 in human breast cancer cell lines. *Oncogene*, **5**, 893–899.
24. Bensaude,O. (2011) inhibiting eukaryotic transcription: Which compound to choose? How to evaluate its activity? *Transcription*, **2**, 103–108.
25. Burger,K., Mühl,B., Harasim,T., Rohrmoser,M., Malamoussi,A., Orban,M., Kellner,M., Gruber-Eber,A., Kremmer,K., Hölzel,M. *et al.* (2010) Chemotherapeutic drugs inhibit ribosome biogenesis at various levels. *J. Biol. Chem.*, **285**, 12416–12425.
26. Lam,Y.W. and Lamond,A.I. (2006) Isolation of nucleoli. In: Celis,JE (ed). *Cell Biology: a Laboratory Handbook*. 3rd edn. Elsevier Academic Press, Cambridge, Massachusetts, Vol. **2**, pp. 103–108.
27. Scott,M.S., Troshin,P.V. and Barton,G.J. (2011) NoD: a nucleolar localization sequence detector for eukaryotic and viral proteins. *BMC Bioinformatics*, **12**, 1–7.
28. Lee,T.I., Johnstone,S.E. and Young,R.A. (2006) Chromatin immunoprecipitation and microarray-based analysis of protein location. *Nat. Protoc.*, **1**, 729–748.
29. O'Sullivan,A.C., Sullivan,G.J. and McStay,B. (2002) UBF binding in vivo is not restricted to regulator sequences within the vertebrate ribosomal DNA repeat. *Mol. Cell Biol.*, **22**, 657–668.
30. Wang,L. and Brown,S.J. (2006) BindN: a web-based tool for efficient prediction of DNA and RNA binding sites in amino acid sequences. *Nucleic Acids Res.*, **34**, W243–W248.
31. Terribilini,M., Sander,J.D., Lee,J.H., Zaback,P., Jernigan,R.L., Honavar,V. and Dobbs,D. (2007) RNABindR: a server for analyzing

and predicting RNA-binding sites in proteins. *Nucleic Acids Res.*, **35**, W578–W584.
32. Obrdlik,A., Louvet,E., Kukalev,A., Naschekin,D., Kiseleva,E., Fahrenkrog,B. and Percipalle,P. (2010) Nuclear myosin 1 is in complex with mature rRNA transcripts and associates with the nuclear pore basket. *FASEB J.*, **24**, 146–157.
33. Philimonenko,V.V., Zhao,J., Iben,S., Dingová,H., Kyselá,K., Kahle,M., Zentgraf,H., Hofmann,W.A., de Lanerolle,P., Hozák,P. *et al.* (2004) Nuclear actin and myosin I are required for RNA polymerase I transcription. *Nat. Cell Biol.*, **6**, 1165–1172.
34. Li,L.Y., Chen,H., Hsieh,Y.H., Wang,Y.N., Chu,H.J., Chen,Y.H., Chen,H.Y., Chien,P.J., Ma,H.T., Tsai,H.C. *et al.* (2011) Nuclear ErbB2 enhances translation and cell growth by activating transcription of ribosomal RNA genes. *Cancer Res.*, **71**, 4269–4279.
35. Lyng,M.B., Laenkholm,A.V., Pallisgaard,N. and Ditzel,N.J. (2008) Identification of genes for normalization of real-time RT-PCR data in breast carcinomas. *BMC Cancer*, **8**, 1–11.
36. Sarshad,A., Sadeghifar,F., Louvet,E., Mori,R., Böhm,S., Al-Muzzaini,B., Vintermist,A., Fomproix,N., Östlund,A.K. and Percipalle,P. (2013) Nuclear myosin 1c facilitates the chromatin modifications required to activate rRNA gene transcription and cell cycle progression. *PLoS Genet.*, **9**, e1003397.
37. Thiry,M. and Lafontaine,D.L. (2005) Birth of a nucleolus: the evolution of nucleolar compartments. *Trends Cell Biol.*, **15**, 194–199.
38. Boisvert,F.M., van Koningsbruggen,S., Navascués,J. and Lamond,A.I. (2007) The multifunctional nucleolus. *Nat. Rev. Mol. Cell Biol.*, **8**, 574–585.
39. de Melo,I.S., Jimenez-Nuñez,M.D., Iglesias,C., Campos-Caro,A., Moreno-Sanchez,D., Ruiz,F.A. and Bolívar,J. (2013) NOA36 protein contains a highly conserved nucleolar localization signal capable of directing functional proteins to the nucleolus, in mammalian cells. *PLoS One*, **8**, e59065.
40. Emmott,E. and Hiscox,J.A. (2009) Nucleolar targeting: the hub of the matter. *EMBO Rep.*, **10**, 231–238.
41. Ochs,R.L., Lischwe,M.A., Spohn,W.H. and Busch,H. (1985) Fibrillarin: a new protein of the nucleolus identified by autoimmune sera. *Biol. Cell*, **54**, 123–133.
42. Westendorf,J.M., Konstantinov,K.N., Wormsley,S., Shu,M.D., Matsumoto-Taniura,N., Pirollet,F., Klier,F.G., Gerace,L. and Baserga,S.J. (1998) M phase phosphoprotein 10 is a human U3 small nucleolar ribonucleoprotein component. *Mol. Biol. Cell*, **9**, 437–449.
43. Chen,H.K., Pai,C.Y., Huang,J.Y. and Yeh,N.H. (1999) Human Nopp140, which interacts with RNA polymerase I: implications for rRNA gene transcription and nucleolar structural organization. *Mol. Cell. Biol.*, **19**, 8536–8546.
44. Bernardi,R., Scaglioni,P.P., Bergmann,S., Horn,H.F., Vousden,K.H. and Pandolfi,P.P. (2004) PML regulates p53 stability by sequestering Mdm2 to the nucleolus. *Nat. Cell Biol.*, **6**, 665–672.
45. Vintermist,A., Böhm,S., Sadeghifar,F., Louvet,E., Mansén,A., Percipalle,P. and Ostlund Farrants,A.K. (2011) The chromatin remodelling complex B-WICH changes the chromatin structure and recruits histone acetyl-transferases to active rRNA genes. *PLoS One*, **6**, e19184.
46. Ye,J., Zhao,J., Hoffmann-Rohrer,U. and Grummt,I. (2008) Nuclear myosin I acts in concert with polymeric actin to drive RNA polymerase I transcription. *Genes Dev.*, **22**, 322–330.
47. Bouvet,P., Diaz,J.J., Kindbeiter,K., Madjar,J. and Amalric,F. (1998) Nucleolin interacts with several ribosomal proteins through its RGG domain. *J. Biol. Chem.*, **273**, 19025–19029.
48. Ginisty,H., Amalric,F. and Bouvet,P. (1998) Nucleolin functions in the first step of ribosomal RNA processing. *EMBO J.*, **17**, 1476–1486.
49. Cong,R., Das,S., Ugrinova,I., Kumar,S., Mongelard,F., Wong,J. and Bouvet,P. (2012) Interaction of nucleolin with ribosomal RNA genes and its role in RNA polymerase I transcription. *Nucleic Acids Res.*, **40**, 9441–9454.
50. Ugrinova,I., Monier,K., Ivaldi,C., Thiry,M., Storck,S., Mongelard,F. and Bouvet,P. (2007) Inactivation of nucleolin leads to nucleolar disruption, cell cycle arrest and defects in centrosome duplication. *BMC Mol. Biol.*, **8**, 1–16.
51. Takagi,M., Absalon,M.J., McLure,K.G. and Kastan,M.B. (2005) Regulation of p53 translation and induction after DNA damage by ribosomal protein L26 and nucleolin. *Cell*, **123**, 49–63.
52. Holmberg Olausson,K., Nistér,M. and Lindström,M.S. (2012) p53-dependent and -independent nucleolar stress responses. *Cells*, **1**, 774–798.
53. Lim,L.Y., Vidnovic,N., Ellisen,L.W. and Leong,C.O. (2009) Mutant p53 mediates survival of breast cancer cells. *Br. J. Cancer*, **101**, 1606–1612.
54. Silk,A.D., Holland,A.J. and Cleveland,D.W. (2009) Requirements for NuMA in maintenance and establishment of mammalian spindle poles. *J. Cell Biol.*, **184**, 677–690.
55. Xu,X., Duan,X., Lu,C., Lin,G. and Lu,G. (2011) Dynamic distribution of NuMA and microtubules in human fetal fibroblasts, developing oocytes and somatic cell nuclear transferred embryos. *Hum. Reprod.*, **26**, 1052–1060.
56. Tabellini,G., Riccio,M., Baldini,G., Bareggi,R., Billi,A.M., Grill,V., Narducci,P. and Martelli,A.M. (2001) Further considerations on the intranuclear distribution of HMGI/Y proteins. *Ital. J. Anat. Embryol.*, **106**, 251–260.
57. Harborth,J., Weber,K. and Osborn,M. (2000) GAS41, a highly conserved protein in eukaryotic nuclei, binds to NuMA. *J. Biol. Chem.*, **275**, 31979–31985.
58. Yang,C.H., Lambie,E.J. and Snyder,M. (1992) NuMA: an unusually long coiled-coil related protein in the mammalian nucleus. *J. Cell Biol.*, **116**, 1303–1317.
59. Ludérus,M.E., den Blaauwen,J.L., de Smit,O.J., Comtpon,D.A. and Driel,R. (1994) Binding of matrix attachment regions to lamin polymers involves single-stranded regions and the minor groove. *Mol. Cell. Biol.*, **14**, 6297–6305.
60. Gallini,S., Carminati,M., De Mattia,F., Pirovano,L., Martini,E., Oldani,A., Asteriti,I.A., Guarguaglini,G. and Mapelli,M. (2016) NuMA phosphorylation by Aurora-A orchestrates spindle orientation. *Curr. Biol.*, **26**, 458–469.
61. Kotak,S. and Gönczy,P. (2014) NuMA phosphorylation dictates dynein-dependent spindle positioning. *Cell Cycle*, **13**, 177–178.
62. Kotak,S., Busso,C. and Gönczy,P. (2013) NuMA phosphorylation by CDK1 couples mitotic progression with cortical dynein function. *EMBO J.*, **32**, 2517–2529.
63. Toughiri,R., Li,X., Du,Q. and Bieberich,C.J. (2013) Phosphorylation of NuMA by Aurora-A kinase in PC-3 prostate cancer cells affects proliferation, survival, and interphase NuMA localization. *J. Cell Biochem.*, **114**, 823–830.
64. Saredi,A., Howard,L. and Compton,D.A. (1997) Phosphorylation regulates the assembly of NuMA in a mammalian mitotic extract. *J. Cell Sci.*, **110**, 1287–1297.
65. Sparks,C.A., Fey,E.G., Vidair,C.A. and Doxsey,S.J. (1995) Phosphorylation of NuMA occurs during nuclear breakdown and not mitotic spindle assembly. *J. Cell Sci.*, **108**, 3389–3396.
66. Compton,D.A. and Luo,C. (1995) Mutation of the predicted p34cdc2 phosphorylation sites in NuMA impair the assembly of the mitotic spindle and block mitosis. *J. Cell Sci.*, **108**, 621–633.
67. Magescas,J., Sengmanivong,L., Viau,A., Mayeux,A., Dang,T., Burtin,M., Nilsson,U.J., Leffler,H., Poirier,F., Terzi,F. *et al.* (2017) Spindle pole cohesion requires glycosylation-mediated localization of NuMA. *Sci. Rep.*, **7**, 1–14.
68. Seo,J.S., Kim,H.N., Kim,S.J., Bang,J., Kim,E.A., Sung,K.S., Yoon,H.J., Yoon,H.Y. and Choi,C.Y. (2014) Cell cycle-dependent SUMO-1 conjugation to nuclear mitotic apparatus protein (NuMA). *Biochem. Biophys. Res. Commun.*, **443**, 259–265.
69. Yan,K., Li,L., Wang,X., Hong,R., Zhang,Y., Yang,H., Lin,M., Zhang,S., He,Q., Zheng,D. *et al.* (2015) The deubiquitinating enzyme complex BRISC is required for proper mitotic spindle assembly in mammalian cells. *J. Cell Sci.*, **210**, 209–224.
70. Russo,A., Pagliara,V., Albano,F., Esposito,D., Sagar,V., Loreni,F., Irace,C., Santamaria,R. and Russo,G. (2016) Regulatory role of rpL3 in cell response to nucleolar stress induced by Act D in tumor cells lacking functional p53. *Cell Cycle*, **16**, 41–51.
71. Esposito,D., Crescenzi,E., Sagar,V., Loreni,F., Russo,A. and Russo,G. (2014) Human rpL3 plays a crucial role in cell response to nucleolar stress induced by 5-Fu and L-OHP. *Oncotarget*, **5**, 11737–11751.
72. Li,J., Yu,L., Zhang,H., Wu,J., Yuan,J., Li,X. and Li,M. (2009) Down-regulation of pescadillo inhibits proliferation and tumorigenicity of breast cancer cells. *Cancer Sci.*, **100**, 2255–2260.
73. Iadevaia,V., Caldarola,S., Biondini,L., Gismondi,A., Karlsson,S., Dianzani,I. and Loreni,F. (2010) PIM1 kinase is destabilized by

ribosomal stress causing inhibition of cell cycle progression. *Oncogene*, **29**, 5490–5499.
74. Ghoshal,K. and Jacob,S.T. (1996) Heat shock selectively inhibits ribosomal RNA gene transcription and down-regulates E1BF/Ku in mouse lymphosarcoma cells. *Biochem. J.*, **317**, 689–695.
75. Mekhail,K., Rivero-Lopez,L., Khacho,M. and Lee,S. (2006) Restriction of rRNA Synthesis by VHL maintains energy equilibrium under hypoxia. *Cell Cycle*, **5**, 2401–2413.
76. Mironova,A.A., Barykina,N.V. and Zatsepina,O.V. (2014) Cytological analysis of the response of nucleolar RNA and RNA-binding proteins to oxidative stress in HeLa cells. *Tsitologiia*, **56**, 489–499.
77. Mayer,C., Bierhoff,H. and Grummt,I. (2005) The nucleolus as a stress sensor: JNK2 inactivates the transcription factor TIF-1A and down-regulates rRNA synthesis. *Genes Dev.*, **19**, 933–941.
78. Han,J., Xu,X., Qin,H., Liu,A., Fan,Z., Kang,L., Fu,J., Liu,J. and Ye,Q. (2013) The molecular mechanism and potential role of heat shock-induced p53 protein accumulation. *Mol. Cell Biochem.*, **378**, 161–169.
79. Lamonte,G., Tang,X., Chen,J.L., Wu,J., Ding,C.K, Keenan,M.M., Sangokoya,C., Kung,H.N., Ilkayeva,O., Boros,L.G. *et al.* (2013) Acidosis induces reprogramming of cellular metabolism to mitigate oxidative stress. *Cancer Metab.*, **1**, 1–19.
80. Zhou,N., Lin,X., Dong,W., Huang,W., Jiang,W., Lin,L., Qiu,Q., Zhang,X., Shen,J., Song,Z. *et al.* (2016) SIRT1 alleviates senescence of degenerative human intervertebral disc cartilage endo-plate cells via the p53/p21 pathway. *Sci. Rep.*, **6**, 1–12.
81. Quintos,L., Lee,I.A., Kim,H.J., Lim,J.S., Park,J., Sung,M.K., Seo,Y.R. and Kim,J.S. (2010) Significance of p27kip1 as potential biomarker for intracellular oxidative status. *Nutr. Res. Pract.*, **4**, 351–355.
82. Harvat,B.L., Wang,A., Seth,P. and Jetten,A.M. (1998) Up-regulation of p27Kip1, p21WAF1/Cip1 and p16Ink4a is associated with, but not sufficient for, induction of squamous differentiation. *J. Cell Sci.*, **111**, 1185–1196.
83. Quaroni,A., Tian,J.Q., Seth,P. and Ap Rhys,C. (2000) $p27^{Kip1}$ is an inducer of intestinal epithelial cell differentiation. *Am. J. Physiol. Cell Physiol.*, **279**, C1045–C1057.
84. Deschênes,C., Vézina,A., Beaulieu,J.F. and Rivard,N. (2001) Role of $p27^{Kip1}$ in human intestinal cell differentiation. *Gastroenterology*, **120**, 423–438.
85. Muñoz-Alonso,M.J., Acosta,J.C., Richard,C., Delgado,M.D., Sedivy,J. and León,J. (2005) $p21^{Cip1}$ and $p27^{Kip1}$ induce distinct cell cycle effects and differentiation programs in myeloid leukemia cells. *J. Biol. Chem.*, **280**, 18120–18129.
86. Nguyen,L., Besson,A., Heng,J.I., Schuurmans,C., Teboul,L., Parras,C., Philpott,A., Roberts,J.M. and Guillemot,F. (2006) $p27^{kip1}$ independently promotes neuronal differentiation and migration in the cerebral cortex. *Genes Dev.*, **20**, 1511–1524.
87. Huleatt,J.W., Cresswell,J., Bottomly,K. and Crispe,I.N. (2003) $P27^{kip1}$ regulates the cell cycle arrest and survival of activated T lymphocytes in response to interleukin-2 withdrawal. *Immunology*, **108**, 493–501.
88. Cassimere,E.K., Mauvais,C. and Denicourt,C. (2016) $p27^{Kip1}$ is required to mediate a G1 cell cycle arrest downstream of ATM following genotoxic stress. *PLoS One*, **11**, e0162806.
89. Zou,P., Yoshihara,H., Hosokawa,K., Tai,I., Shinmyozu,K., Tsukahara,F., Maru,Y., Nakayama,K., Nakayama,K.I. and Suda,T. (2011) p57(Kip2) and p27(Kip1) cooperate to maintain hematopoietic stem cell quiescence through interactions with Hsc70. *Cell Stem Cell*, **9**, 247–261.
90. Oesterle,E.C., Chien,W.M., Campbell,S., Nellimarla,P. and Fero,M.L. (2011) p27(Kip1) is required to maintain proliferative quiescence in the adult cochlea and pituitary. *Cell Cycle*, **10**, 1237–1248.
91. Zhang,J., Seet,C.S., Sun,C., Li,J., You,D., Volk,A., Breslin,P., Li,X., Wei,W., Qian,Z. *et al.* (2013) $p27^{kip1}$ maintains a subset of leukemia stem cells in the quiescent state in murine MLL-leukemia. *Mol. Oncol.*, **7**, 1069–1082.
92. Lakin,N.D. and Jackson,S.P. (1999) Regulation of p53 in response to DNA damage. *Oncogene*, **18**, 7644–7655.
93. Krüger,T and Scheer,U. (2010) p53 localizes to intranucleolar regions distinct from the ribosome production compartments . *J. Cell Sci.*, **123**, 1203–1208.
94. Lu,K., Wang,J., Song,Y., Zhao,S., Liu,H., Tang,D., Pan,B., Zhao,H. and Zhang,Q. (2015). miRNA-24-3p promotes cell proliferation and inhibits apoptosis in human breast cancer by targeting p27Kip1. *Oncol. Rep.*, **34**, 995–1002.
95. Catzavelos,C., Bhattacharya,N., Ung,Y.C., Wilson,J.A., Roncari,L., Sandhu,C., Shaw,P., Yeger,H., Morava-Protzner,I., Kapusta,L. *et al.* (1997) Decreased levels of the cell-cycle inhibitor p27kip1 protein: prognostic implications in primary breast cancer. *Nat. Med.*, **3**, 227–230.
96. Viglietto,G., Motti,M.L. and Fusco,A. (2002) Understanding p27kip1 deregulation in cancer: downregulation or mislocalizaiton. *Cell Cycle*, **1**, 394–400.
97. Orsolic,I., Jurada,D., Pullen,N., Oren,M., Eliopoulos,A.G. and Volarevic,S. (2006). The relationship between the nucleolus and cancer: Current evidence and emerging paradigms. *Semin. Cancer Biol.*, **37–38**, 36–50.
98. Yoon,A., Peng,G., Brandenburger,Y., Zollo,O., Xu,W., Rego,E. and Ruggero,D. (2006) Impaired control of IRES-mediated translation in X-linked dyskeratosis congenita. *Science*, **312**, 902–906.
99. Bursac,S., Brdovcak,M.C., Donati,G. and Volarevic,S. (2014) Activation of the tumor suppressor p53 upon impairment of ribosome biogenesis. *Biochim. Biophys. Acta.*, **1842**, 817–830.
100. Zannoni,G.F., Faraglia,B., Tarquini,E., Camerini,A., Vrijens,K., Migaldi,M., Cittadini,A. and Sgambato,A. (2006) Expression of the CDK inhibitor p27kip1 and oxidative DNA damage in non-neoplastic and neoplastic vulvar epithelial lesions. *Mod. Pathol.*, **19**, 504–513.